Radboud Repository

Radboud University Nijmegen

PDF hosted at the Radboud Repository of the Radboud University Nijmegen

The following full text is a pre which may differ from the publisher's version.

For additional information about this publication click this link.
http://hdl.handle.net/2066/175428

Please be advised that this information was generated on 2019-06-01 and may be subject to change.

Magnetoresistance of compensated semimetals in confined geometries

P. S. Alekseev,[1] A. P. Dmitriev,[1] I. V. Gornyi,[2, 1] V. Yu. Kachorovskii,[1] B. N. Narozhny,[3, 4] M. Schütt,[5] and M. Titov[6]

[1]*A. F. Ioffe Physico-Technical Institute, 194021 St. Petersburg, Russia*
[2]*Institut für Nanotechnologie, Karlsruhe Institute of Technology, 76021 Karlsruhe, Germany*
[3]*Institut für Theorie der Kondensierten Materie, Karlsruhe Institute of Technology, 76128 Karlsruhe, Germany*
[4]*National Research Nuclear University MEPhI (Moscow Engineering Physics Institute), 115409 Moscow, Russia*
[5]*School of Physics and Astronomy, University of Minnesota, Minneapolis, MN 55455, USA*
[6]*Radboud University Nijmegen, Institute for Molecules and Materials, NL-6525 AJ Nijmegen, The Netherlands*

Two-component conductors – e.g., semi-metals and narrow band semiconductors – often exhibit unusually strong magnetoresistance in a wide temperature range. Suppression of the Hall voltage near charge neutrality in such systems gives rise to a strong quasiparticle drift in the direction perpendicular to the electric current and magnetic field. This drift is responsible for a strong geometrical increase of resistance even in weak magnetic fields. Combining the Boltzmann kinetic equation with sample electrostatics, we develop a microscopic theory of magnetotransport in two and three spatial dimensions. The compensated Hall effect in confined geometry is always accompanied by electron-hole recombination near the sample edges and at large-scale inhomogeneities. As the result, classical edge currents may dominate the resistance in the vicinity of charge compensation. The effect leads to linear magnetoresistance in two dimensions in a broad range of parameters. In three dimensions, the magnetoresistance is normally quadratic in the field, with the linear regime restricted to rectangular samples with magnetic field directed perpendicular to the sample surface. Finally, we discuss the effects of heat flow and temperature inhomogeneities on the magnetoresistance.

The theory of magnetotransport in solids[1,2] is a mature branch of condensed matter physics. Measurements of magnetoresistance and classical Hall effect are long recognized as valuable experimental tools to characterize conducting samples. Interpreting the experiments within the standard Drude theory[1,3,4], one may extract many useful sample characteristics such as the electron mobility and charge density at the Fermi level. However, in materials with more than one type of charge carriers – e.g., semimetals and narrow band semiconductors – the situation is more complex. Indeed, already in 1928 Kapitsa observed unconventional magnetoresistance in semi-metal bismuth films[5]. More recently, interest in magnetotransport has been revived with the discovery of novel two-component systems including graphene[6–11], topological insulators[12–16], and Weyl semimetals[17–27]. A common feature of all such systems is the existence of the charge neutrality (or, charge compensation) point, where the concentrations of the positively and negatively charged quasiparticles (electron-like and hole-like, respectively) are equal and the system is electrically neutral.

A fast growing number of experiments on novel two-component materials exhibit unconventional transport properties in magnetic field: (i) linear magnetoresistance (LMR) was reported in graphene and topological insulators close to charge neutrality[28–36] as well as in narrow-gap semiconductors[37], bismuth films[38,39], and three-dimensional (3D) silver chalcogenides[40–42] (ii) giant (and sometimes also linear) magnetoresistance was identified in semimetals WTe[43–45], NbP[46], $LaBi$[47,48], $ZrSiS$[49,50], multilayer graphene[51] and many others[52–57]; (iii) finally, the widely discussed negative magnetoresistance was found in Weyl semimetals and related materials[58–68]. Moreover, negative magnetoresistance may by regarded as a "smoking gun" for detecting a Weyl semimetal[69,70],

although experiment[71,72] shows the existence of the effect in "non-Dirac" materials as well.

Conventional Drude-like theories of transport in two-component systems predict parabolic magnetoresistance that saturates in classically strong fields[1,3,73,74]. Taking into account additional relaxation processes may lead to semiclassical mechanisms of LMR in diverse physical systems including 3D metallic slabs with complex Fermi surfaces and smooth boundaries[75,76]; strongly inhomogeneous or granular materials[77–80]; short samples[80,81]; disordered 3D metals[82,83]; and compensated two-component systems[84]. Quantum effects result in LMR in strong fields in 3D zero-gap band systems with linear dispersion[85–87]. In weak fields, resistivity of two-dimensional (2D) electron systems acquires an interaction correction[88] that is linear in the field.

The extreme quantum limit of Refs. 85–87 has been realized in graphene[28], Bi_2Te_3 nanosheets[56], and possibly in the novel topological material $LuPdBi$[57]. However, this mechanism is applicable to the specific case of 3D systems with linear dispersion subjected to a strong magnetic field $\hbar\omega_c \gg T$ (as usual, T is the temperature, $\hbar$ is the Planck constant, and ω_c is the electron cyclotron frequency), where all electrons are confined to the first Landau level. Recently, this approach has been extended to Weyl semimetals at finite temperatures and with short-range disorder[89]. However, the above conditions are typically not satisfied by the majority of systems exhibiting unsaturated LMR at high temperatures.

Experiments on strongly inhomogeneous (or strongly disordered) systems are often interpreted using the classical approach of Refs. 77,78. In particular, the random-resistor model of Ref. 78 was introduced to explain the non-saturating LMR in granular materials such as $AgSe$[40,41]. More recently, this mechanism was used to

interpret the behavior of the hydrogen-intercalated epitaxial bilayer graphene[33]. However, this model (as well as the quantum theory of Refs. 85–87) does not distinguish between single- and multi-component systems, contradicting the crucial role of the charge neutrality point in many aforementioned experiments. Moreover, both theoretical approaches rely on the presence of disorder and thus cannot be used to interpret the data obtained in ultra-clean, homogeneous samples.

A phenomenological theory of magnetotransport in 2D clean, two-component systems close to charge neutrality was proposed by the present authors in Ref. 84. Subjected to a perpendicular magnetic field, such systems exhibit the compensated Hall effect, where the Hall voltages due to positively and negatively charged carriers partially (precisely at charge neutrality – completely) cancel each other. Such compensation of the Hall voltage is accompanied by a neutral quasiparticle flow in the lateral direction relative to the electric current[90]. In constrained geometries this leads to a nonuniform distribution of charge carriers over the sample area, effectively splitting the sample into the bulk and edge regions. The resistance of the edge region is dominated by the electron-hole recombination, while the bulk of the sample exhibits the usual, essentially Drude resistance. The total resistance of the sample is then obtained by treating the edge and bulk regions as independent, parallel resistors. The linear dependence of the sample resistance on the magnetic field arises due to qualitatively different behavior of the edge region. At charge neutrality, the resulting LMR persists into the range of classically strong fields. Away from the neutrality point, the nonzero Hall voltage leads to the observed saturation of the magnetoresistance. Similar ideas were recently exploited by some of us to explain the phenomenon of the giant magnetodrag in graphene[90,91]. The importance of the electron-hole recombination processes for magnetotransport in narrow-band semiconductors and semimetals has been pointed out earlier by Rashba *et. al.* in Ref. 92.

In this paper we present a microscopic theory of magnetotransport in two-component systems. Combining the kinetic equation with the sample electrostatics, we provide a rigorous justification for the phenomenological approach of Ref. 84. Furthermore, we extend our theory to 3D systems. We find that although in 3D the magnetoresistance is typically quadratic in the field, there exists a linear regime in rectangular samples with magnetic field directed perpendicular to the sample surface.

The remainder of the paper is organized as follows. First, we discuss the qualitative physics of magnetotransport in two-component systems. In the technical part of the paper we present a Boltzmann equation approach to magnetotransport in finite-size 2D and 3D systems. In the latter case, we focus on the rectangular sample geometry to simplify the analysis of the sample electrostatics. We conclude the paper by discussing the experimental relevance of our results.

I. QUALITATIVE DISCUSSION

Let us first recall the results of the classical linear response theory[1,3,4,73,74] applied to two-component systems. A system of charge carriers subjected to a homogeneous external electric field, $\boldsymbol{E}$ exhibits an electrical current. The current density, $\boldsymbol{J} = e\boldsymbol{j}$, is proportional to the applied field, $J_\alpha = \sigma^{\alpha\beta}E_\beta$, where $\hat{\sigma}$ is the conductivity tensor. In two-component systems, one can define currents for each individual carrier subsystems, which we will refer to as electron and hole quasiparticle flows, $\boldsymbol{j}_e$ and $\boldsymbol{j}_h$, respectively. The electric current is then given by their difference, $\boldsymbol{j} = \boldsymbol{j}_h - \boldsymbol{j}_e$.

In external magnetic field, the system exhibits the classical Hall effect: a voltage is generated across the system in the transverse direction to the electric current. In a typical transport measurement, external leads are attached to the sample in such a way, that no current is allowed to flow in the direction of the Hall voltage. Theoretical description of the effect is most transparent in isotropic systems, where $\sigma^{\alpha\beta} = \sigma_0\delta^{\alpha\beta}$. If we associate the x-axis with the electric current and the z-axis with the magnetic field, then the Hall voltage is generated in the y direction, while $J_y = 0$. In two-component systems, the latter condition leads to a field-dependent longitudinal resistivity[73,74]

$$\rho^{xx} = \frac{1}{\sigma_0} \frac{\sigma_0^2 + \tilde{\sigma}_0^2 \mu_e \mu_h B^2}{\sigma_0^2 + e^2(n_{0,e} - n_{0,h})^2 \mu_e^2 \mu_h^2 B^2}, \qquad (1)$$

where B is the magnetic field, $n_{0,e}$ and $n_{0,h}$ stand for the equilibrium electron and hole densities, and μ_e and μ_h are the electron and hole mobilities. Within the standard Drude theory[1,3,4], the conductivity σ_0 can be expressed in terms of the quasiparticle densities and mobilities as

$$\sigma_0 = e n_{0,e} \mu_e + e n_{0,h} \mu_h,$$

whereas the additional parameter $\tilde{\sigma}_0$ is

$$\tilde{\sigma}_0 = e\sqrt{\mu_e \mu_h (n_{0,e}^2 + n_{0,h}^2) + n_{0,e} n_{0,h}(\mu_e^2 + \mu_h^2)}.$$

In the presence of the electron-hole symmetry, the mobilities of the two types of carriers coincide, $\mu_e = \mu_h = \mu$, and the resistivity (1) simplifies to

$$\rho^{xx} = \frac{\rho_0}{e\mu} \frac{1 + (\mu B)^2}{\rho_0^2 + n_0^2(\mu B)^2}, \qquad (2)$$

where we have introduced quasiparticle and charge densities, $\rho_0 = n_{0,e} + n_{0,h}$ and $n_0 = n_{e,0} - n_{h,0}$, respectively.

The results (1) and (2) yield a positive magnetoresistance that is quadratic in weak magnetic fields and saturates in classically strong fields. The two exceptions are provided by neutral systems ($n_0 = 0$, $n_{0,e} = n_{0,h}$), where the quadratic magnetoresistance is non-saturating, and single-component systems (e.g. for purely electronic transport $n_0 = \rho_0 = n_{0,e}$, $n_{0,h} = 0$), where the longitudinal resistivity is independent of the magnetic field[1,3,4].
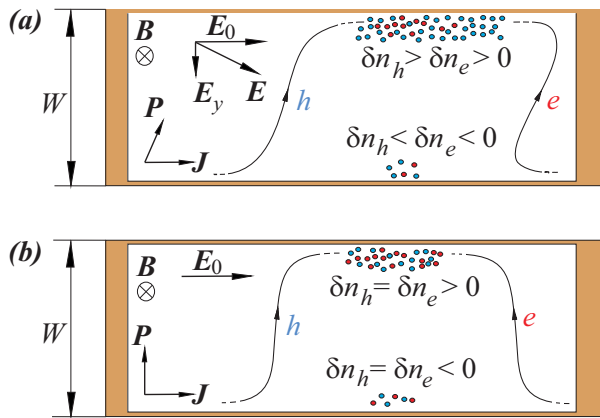
FIG. 1: Typical semiclassical trajectories for oppositely charged quasiparticles in two-component systems at charge neutrality. The two panels illustrate electron-hole asymmetric (a) and symmetric (b) systems. As a manifestation of the compensated Hall effect, both quasiparticle currents are flowing in the same direction in the bulk of the sample. In the symmetric sample (b), the quasiparticle flow, $\boldsymbol{P} = \boldsymbol{j}_e + \boldsymbol{j}_h$, is orthogonal to the electric current. In the asymmetric case (a), the longitudinal component of $\boldsymbol{P}$ is also finite. Such a flow leads to quasiparticle accumulation at the boundaries of the otherwise homogeneous sample. The excess quasiparticle density appears in a boundary region of the width of the order of the electron-hole recombination length. Contributions of the bulk and boundary regions to the sheet resistance exhibit different dependence on the magnetic field. In classically strong fields, the boundary region may dominate leading to linear magnetoresistance.
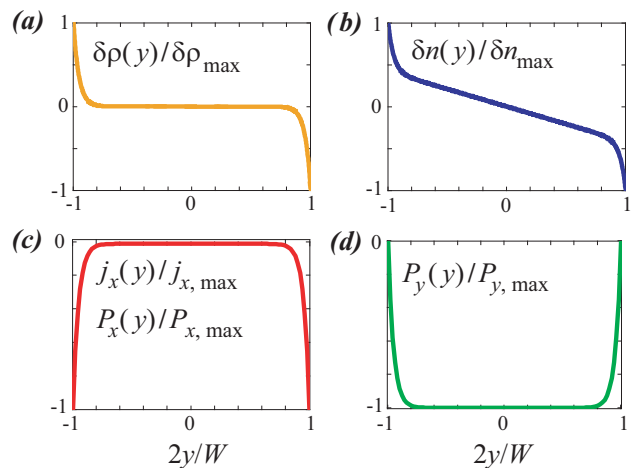

FIG. 2: Lateral profiles of the quasiparticle density $\delta\rho(y)$, charge density $\delta n(y)$, quasiparticle flow $P_{x,y}(y)$ and electric current density $J_x(y)$ in a 2D two-component system away from charge neutrality, see Fig. 1, panel (a), calculated within the theory presented in Sec. II. For concreteness, we chose the carrier parameters of a typical topological-insulator film: electron and hole mobilities $\mu_e = 20\mu_h$, $\mu_h = 1 \ \mathrm{m}^2/(\mathrm{V\cdot s})$ and velocities $v_e = 10^6$ m/s, $v_h = 0.5v_e$. The sample is assumed have the width $W = 10\mu m$, with the distance to the gate $d = 0.5\mu m$ and the dielectric constant of the surrounding insulator $\epsilon = 5$. The carrier densities were calculated using a generic two-band model with the energy gap $\Delta = 4$ meV at room temperature $T = 300$ K. The recombination length is assumed to take the value $\ell_R = 0.46\mu m$ at $B = 2$ T. All curves are normalized to the maxima of their absolute values.

Previously[84,90], we have pointed out an inconsistency that appears when the above classical theory is applied to finite-sized samples. Indeed, even partially compensated Hall effect is accompanied by a neutral quasiparticle flow in the direction transversal to that of the electrical current, see Figs. 1 and 2. As the quasiparticles cannot leave the sample, this flow leads to quasiparticle accumulation near the sample boundaries. The excess quasiparticle density is controlled by inelastic recombination processes that are excluded from the classical theory. The typical length scale characterizing such processes, ℓ_R, hereafter referred to as the recombination length, determines the size of the boundary region with excess density of quasiparticles. Here we consider rectangular samples with the length L being the longest length scale in the system[93],

$$\ell_R, \ell_R\mu B, W \ll L. \qquad (3)$$

The classical results are applicable if the boundary regions are small as compared to the sample width, $\ell_R \ll W$. If, on the other hand, ℓ_R is comparable with W, then the behavior of the system may strongly deviate from the predictions of the classical theory.

Treating the bulk and boundary regions as parallel conductors, we estimate the sheet resistance of the sample[84]

$$R_\square = \frac{W}{L} \frac{1}{R_{\mathrm{bulk}}^{-1} + R_{\mathrm{edge}}^{-1}}. \qquad (4)$$

In the bulk, the lateral quasiparticle flow leads to the so-called "geometric" magnetoresistance[94,95]

$$R_{\mathrm{bulk}} \approx \frac{L}{W}\rho^{xx} \quad \Rightarrow \quad R_{\mathrm{bulk}}^{-1} \approx \frac{W}{L}e\mu\rho_0\left[\frac{n_0^2}{\rho_0^2} + \frac{1}{\mu^2 B^2}\right],$$

where we have used Eq. (2) in the limit of classically strong magnetic fields, $\mu B \gg 1$.

In the boundary regions, the quasiparticle flows are mostly directed along the external electric field, see Figs. 1 and 2, and the geometric enhancement does not take place. Instead, the field dependence of the edge contribution to the sample resistance,

$$R_{\mathrm{edge}} \approx \frac{L}{\ell_R}\rho^{xx}(B = 0),$$

is due to the recombination length, ℓ_R. In homogeneous samples, the simplest estimate[84,90] yields ℓ_R that is inverse proportional to B in classically strong fields

$$\ell_R = \frac{\ell_0}{\sqrt{1 + \mu^2 B^2}} \rightarrow \frac{\ell_0}{\mu B}, \qquad (5)$$

where $\ell_0 = 2\sqrt{D\tau_R}$ is the zero-field recombination length determined by the diffusion coefficient D and the characteristic recombination time τ_R.

The asymptotic behavior (5) of the recombination length may be qualitatively understood as follows. In classically strong magnetic fields, $\mu B \gg 1$, the charge carriers move over a typical distance R_c (the cyclotron radius) during a typical diffusion time τ. Since the quasi-particle life-time is determined by the recombination processes, the overall distance covered by the electron during the time τ_R may not exceed $R_c\sqrt{\tau_R/\tau} \sim 1/B$, which yields the estimate for the size of the boundary regions.

Combining the above arguments, we arrive at the following expression for the sheet resistance (4) in classically strong magnetic fields, $\mu B \gg 1$,

$$R_\square = \frac{1}{e\rho_0\mu}\left[\frac{n_0^2}{\rho_0^2} + \frac{1}{\mu^2 B^2} + \frac{\ell_0}{\mu B W}\right]^{-1}. \qquad (6)$$

The sheet resistance (6) exhibits all qualitative features of the magnetoresistance in nearly compensated two-component systems.

In *wide samples*, $W \gg \ell_0 \mu B$, magnetotransport is dominated by the bulk and can be described by the classical theory, see Eqs. (1) and (2) and the subsequent discussion. We consider such samples as essentially infinite.

Deviations from the classical behavior (1) and (2) occurs in finite-size samples of the width belonging to the *intermediate* interval determined by the magnetic field,

$$\frac{\ell_0}{\mu B} \ll W \ll \mu B \ell_0.$$

In this case, the sheet resistance of compensated (neutral, $n_0 = 0$) systems is linear in the magnetic field

$$R_\square = \frac{1}{e\rho_0}\frac{W}{\ell_0}B. \qquad (7)$$

Away from charge neutrality, LMR appears only in an intermediate range of magnetic fields. In strong fields, $B \gtrsim \ell_0\rho_0^2/(\mu W n_0^2)$, magnetoresistance saturates.

In *narrow samples*, $W \ll \ell_R \sim \ell_0/\mu B$, recombination is ineffective and the above physical picture breaks down. In this case, the two carrier subsystems behave as two independent single-component systems. As a consequence, classical magnetoresistance is absent[1,3,4].

The sheet resistance (6) is illustrated in Fig. 3 where it is plotted in a wide range of classically strong magnetic fields in the above three regimes. Panel (a) shows $R_\square$ for a symmetric system at charge neutrality, while panels (b), (c), and (d) illustrate our results for asymmetric systems at (solid curves) and away from (dashed curves) the compensation point.

The above semiclassical mechanism of LMR in finite-size, nearly compensated two-component system was first suggested in Ref. 90 in the context of Coulomb drag[91]. The results (4)-(7) were derived rigorously in graphene[98] on the basis of a microscopic transport theory. Subsequently, the macroscopic equations derived in graphene were generalized to a generic compensated two-component system using a phenomenological approach[84].
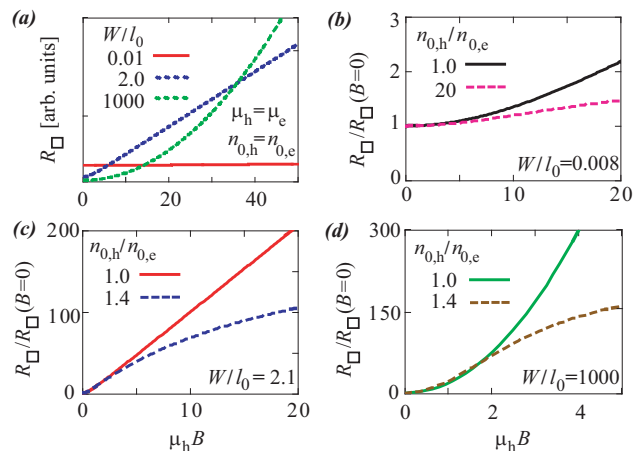

FIG. 3: (a) Sheet resistance $R_\square(B)$ of a 2D symmetric, two-component system at charge neutrality for three different values of the ratio of the sample width to the zero-field recombination length, $W/\ell_0 = 0.01, 2, 1000$, represented by the solid red, dotted blue, and dashed green lines, respectively (the curves are rescaled for clarity). (b), (c), (d) $R_\square(B)$ of a 2D asymmetric two-component system for three different values $W/\ell_0 = 0.008$ [panel (b)], $W/\ell_0 = 2.1$ [panel (b)], and $W/\ell_0 = 1000$ [panel (c)]. In all three plots, solid lines correspond to the charge neutrality point, while dashed lines show results away from neutrality. The curves were calculated using the theory presented in Sec. II, with the parameter values correspond to typical topological-insulator films (see the caption to Fig. 2), with the recombination length $\ell_0 = 4.8\mu m$.

In this paper, we justify the phenomenological approach of Ref. 84 and derive the LMR for a wide range of systems using the Boltzmann kinetic equation. The key point that makes our theory so general, is the simple fact that in an magnetic field charge carriers driven through the system by the external electric field experience a lateral drift in the direction ($\boldsymbol{E} \times \boldsymbol{B}$) defined by the electric and magnetic fields. The ultimate cause of this drift is the Lorenz force that acts on all charge carriers independently of their density, mobility, details of the spectrum, and additional quantum numbers. The second essential feature of our theory is the presence of the boundary leading to accumulation of the excess quasiparticle density in the narrow regions near the sample edges. Again, this is a completely general feature since all samples used in laboratory (as well as all industrial electronic devices) have a finite size. The width of the boundary regions (and hence, the degree of macroscopic inhomogeneity in the system, see Fig. 2) is controlled by the quasiparticle recombination length. The particular dependence (5) of ℓ_R on the magnetic field is crucial for the resulting LMR, given by Eq. (7). The original estimate[84] (5) is not universal[36] insofar that the coefficient of the inverse proportionality $\ell_R \propto 1/B$ (in classically strong fields) is system (or model) dependent. In a sense, the technical goal of the microscopic theory presented in this paper is to calculate the field dependence of the effective recombination length.

In our qualitative arguments, we have tacitly assumed that the energy transfer plays no role in formation of the macroscopic inhomogeneities of the quasiparticle currents and densities. At the microscopic level, this means energy relaxation (and hence, thermalization) in the system is much faster than quasiparticle recombination. As a result, the temperatures of both carrier subsystems are uniform within the sample (and are, in fact, identical).

The theory of Refs. 84,90,98, as well as the present qualitative discussion and the microscopic theory of Sec. II, is focused on 2D systems. Similar behavior can be found also in 3D samples. In particular, if cyclotron orbits do not remove the carriers from a plane parallel to one of the sample faces, a linear regime similar to Eq. (7) may be observed. In this paper, we make the first steps towards a full microscopic understanding of magnetotransport in 3D two-component systems, see Sec. III.

II. TRANSPORT THEORY OF 2D TWO-COMPONENT SYSTEMS

In this Section we show that the linear dependence of resistivity on the sufficiently strong magnetic field is a generic effect for two-component systems at charge neutrality. For brevity, we employ the natural system of units where $\hbar = c = k_B = 1$.

The usual starting point for developing a microscopic transport theory is the kinetic equation[3]. For a generic two-component electronic system, the kinetic equation has the standard form

$$\boldsymbol{v}_\alpha \frac{\partial f_\alpha}{\partial \boldsymbol{r}} + e_\alpha \left(\boldsymbol{E} + \boldsymbol{v}_\alpha \times \boldsymbol{B}\right) \frac{\partial f_\alpha}{\partial \boldsymbol{p}} = \mathrm{St}[f_\alpha]. \qquad (8)$$

The semiclassical distribution functions $f_\alpha = f_\alpha(\varepsilon, \boldsymbol{p}, \boldsymbol{r})$ describe the positively and negatively charged quasiparticles ("holes" and "electrons", respectively, distinguished by the index $\alpha = e, h$) with the energies $\varepsilon_\alpha(\boldsymbol{p})$ and velocities $\boldsymbol{v}_\alpha = \partial \varepsilon_\alpha(\boldsymbol{p})/\partial \boldsymbol{p}$. The system is subjected to the external electric and magnetic fields $\boldsymbol{E}$ and $\boldsymbol{B}$.

The collision integral in the right hand side of Eq. (8) comprises contributions from impurity, electron-phonon, and electron-electron scattering. We will describe these scattering processes by the typical time scales τ_{imp}, τ_{ee}, and τ_{ph}. The impurity and electron-phonon scattering contribute to momentum relaxation, while the electron-electron and electron-phonon interactions determine the thermalization properties of the system, as well as quasiparticle recombination. The traditional transport theory[1,3,4] assumes that in the absence of external fields the system is in equilibrium. The electric current (or more generally, the quasiparticle flows) appears as a response to the applied fields. Within linear response, the system experiences no heating and remains thermalized. In this (and the following) Section we work under the same assumptions.

Finding a general solution to the kinetic equation (8) is a complicated task that is best accomplished numeri-

cally. In the special case of Dirac fermions in graphene, the solution is facilitated by the so-called collinear scattering singularity[98]. Otherwise, an analytical solution can be found in the two paradigmatic limiting cases, known as the "disorder-dominated" and "hydrodynamic" regimes[3,91], which can be distinguished by comparing the scattering rates for elastic and inelastic processes:

(i) in the *disorder-dominated* regime, the fastest scattering process in the system is due to potential disorder,

$$\tau_{\mathrm{imp}} \ll \tau_{\mathrm{ee}}, \tau_{\mathrm{ph}}. \qquad (9)$$

Since the electron-electron scattering time is typically inverse proportional to temperature,

$$\tau_{\mathrm{ee}}^{-1} \propto T,$$

the relation (9) implies

$$T\tau_{\mathrm{imp}} \ll 1,$$

which means that the motion of the charge carriers is diffusive. In this case, most of the transport coefficients can be expressed in terms of the diffusive constant. As a result, qualitative features of the physical observables are independent of the microscopic details, such as the precise form of the single-particle spectrum.

(ii) in the *hydrodynamic* regime, the fastest process is due to electron-electron interaction

$$\tau_{\mathrm{ee}} \ll \tau_{\mathrm{imp}}, \tau_{\mathrm{ph}}. \qquad (10)$$

Now, the relation between the temperature and the impurity scattering time is reversed,

$$T\tau_{\mathrm{imp}} \gg 1,$$

so that the motion of charge carriers is ballistic. In this limit, the system of charged quasiparticles behaves similarly to a fluid and is described by the hydrodynamic equations.

Remarkably, in both regimes the resistance of 2D two-component systems close to charge neutrality exhibits linear dependence on the orthogonal magnetic field (in sufficiently strong fields).

A. Disorder-dominated regime

1. Symmetric, parabolic bands at charge neutrality

We begin with the simplest case of the symmetric parabolic spectrum with the band gap Δ,

$$\varepsilon_e(\boldsymbol{p}) = \varepsilon_h(\boldsymbol{p}) = \varepsilon_{\boldsymbol{p}} = \Delta/2 + p^2/2m, \qquad (11)$$

where the quasiparticle velocity is proportional to the momentum

$$\boldsymbol{v}_\alpha = \boldsymbol{p}_\alpha/m.$$

Furthermore, we will assume the energy-independent momentum relaxation time

$$\tau_h(\varepsilon) = \tau_e(\varepsilon) = \tau = const.$$

At charge neutrality, the equilibrium state of the system is described by the Fermi distribution function with the zero chemical potential

$$f_{\boldsymbol{p}}^{(0)} = \frac{1}{1 + e^{\varepsilon_{\boldsymbol{p}}/T}}.$$

Since the single-particle spectrum (11) depends only on the momentum, the equilibrium quasiparticle density is given by

$$\rho_0 = 2g \int \frac{d^2\boldsymbol{p}}{(2\pi)^2} f_{\boldsymbol{p}}^{(0)}, \qquad (12)$$

where g is the degeneracy factor reflecting other possible quantum numbers, such as spin, valley, etc.

External fields drive the system out of equilibrium, giving rise to deviations of the quasiparticle densities from the equilibrium value (12)

$$\delta n_\alpha = g \int \frac{d^2\boldsymbol{p}}{(2\pi)^2} f_\alpha - \frac{\rho_0}{2}, \qquad (13)$$

and the corresponding flow densities $\boldsymbol{j}_\alpha$:

$$\boldsymbol{j}_\alpha = g \int \frac{d^2\boldsymbol{p}}{(2\pi)^2} \boldsymbol{v} f_\alpha. \qquad (14)$$

The nonequilibrium densities δn_α and currents $\boldsymbol{j}_\alpha$ are related by the continuity equations that can be derived by integrating the kinetic equation (8)

$$\operatorname{div} \boldsymbol{j}_{e(h)} = -\frac{\delta n_h + \delta n_e}{2\tau_R}. \qquad (15)$$

Here τ_R denotes the quasiparticle recombination time. The recombination processes typically involve electron-phonon scattering, although in certain circumstances electron-electron[91] and three-particle[97] collisions may also contribute. A calculation of the recombination time τ_R using a particular microscopic model is beyond the scope of the present paper.

Macroscopic equations[98] for the flow densities (14) can be obtained by multiplying the kinetic equation (8) by the quasiparticle velocity and summing over all single-particle states. As a result, we find[97,98]

$$\boldsymbol{\nabla} \left[g \int \frac{d^2\boldsymbol{p}}{(2\pi)^2} \frac{v^2}{2} f_\alpha \right] - \frac{e_\alpha \boldsymbol{E} \rho_0}{2m} - \boldsymbol{j}_\alpha \times \boldsymbol{\omega}_\alpha = -\frac{\boldsymbol{j}_\alpha}{\tau}, \quad (16)$$

where $\boldsymbol{\omega}_h = -\boldsymbol{\omega}_e = \boldsymbol{\omega}_c$ are the carrier cyclotron frequencies $\boldsymbol{\omega}_c = e\boldsymbol{B}/m$.

Comparing the integral in Eq. (16) with the flow density (14), we find it natural to split the distribution functions f_α into the "isotropic" and "anisotropic" parts,

$$f_\alpha = f_\alpha^{(i)}(\varepsilon) + f_\alpha^{(a)}(\varepsilon, \boldsymbol{e_p}). \qquad (17)$$

The isotropic term depends only on the quasiparticle energy and hence does not contribute to the currents (14). On the contrary, the anisotropic term is an odd function of the momentum. It is this part of the distribution function that determines the currents (14), but at the same time, it does not contribute to the integral in Eq. (16).

Within linear response, deviations of the isotropic function $f_\alpha^{(i)}(\varepsilon)$ from the equilibrium distribution $f_{\boldsymbol{p}}^{(0)}$ can either reflect deviations of the local electronic temperature from the equilibrium value determined by the lattice, or the local fluctuations of the chemical potential $\delta\mu_\alpha(\boldsymbol{r})$.

Thermalization between the electronic system and the lattice is achieved by means of electron-phonon coupling. While the same coupling is also responsible for quasiparticle recombination, the latter is a much slower process and does not affect the local temperature. Relegating a more detailed discussion of this issue to a future publication, hereafter we assume that the relation

$$\tau_{\mathrm{ph}} \ll \tau_R$$

allows us to neglect local temperature fluctuations

$$\delta T(\mathbf{r}) = 0.$$

As a result, the isotropic part of the distribution function may only depend on the local fluctuations of the chemical potential

$$f_\alpha^i = f_{\boldsymbol{p}}^{(0)} + \frac{\partial f_{\boldsymbol{p}}^{(0)}}{\partial \varepsilon} \delta\mu_\alpha(\boldsymbol{r}). \qquad (18)$$

This implies the proportionality between the local density fluctuations (13) and $\delta\mu_\alpha(\boldsymbol{r})$:

$$\delta n_\alpha = \nu_0 \delta\mu_\alpha, \qquad (19)$$

where (cf. Ref. 98)

$$\nu_0 = \langle 1 \rangle, \qquad \langle \cdots \rangle = -g \int_{\Delta/2}^\infty d\varepsilon \nu(\varepsilon) \frac{\partial f^{(0)}}{\partial \varepsilon} (\cdots), \qquad (20)$$

with $\nu(\varepsilon)$ being the density of states [ν_0 has dimensions of $\nu(\varepsilon)$].

Since the equilibrium distribution $f_{\boldsymbol{p}}^{(0)}$ is independent of $\boldsymbol{r}$, we can express the integral in Eq. (16) as

$$g \int \frac{d^2\boldsymbol{p}}{(2\pi)^2} \frac{v^2}{2} f_\alpha = \frac{\langle v^2 \rangle}{2} \delta\mu_\alpha = \frac{\langle v^2 \rangle}{2\nu_0} \delta n_\alpha,$$

and introduce the diffusion coefficient in Eq. (16)

$$D\boldsymbol{\nabla}\delta n_\alpha - e_\alpha \boldsymbol{E} \rho_0 \tau/(2m) - \boldsymbol{j}_\alpha \times \boldsymbol{\omega}_\alpha \tau = -\boldsymbol{j}_\alpha. \qquad (21)$$

The diffusion coefficient is the same for the electrons and holes:

$$D = \langle v^2 \rangle \tau/(2\nu_0). \qquad (22)$$

At charge neutrality the averages in the expression for the diffusion coefficient can be evaluated analytically:

$$D(\mu=0) = \frac{T\tau}{m}\left(1 + e^{\Delta/2T}\right)\ln\left(1 + e^{-\Delta/2T}\right). \quad (23)$$

The macroscopic equations (15) and (21) allow us to find transport coefficients of the system, as well as the carrier density and current profiles. These equations are semiclassical in the sense that the effects of quantum interference[88] and Landau quantization[3,85–87] are neglected.

In this paper we are interested in solving the macroscopic transport equations (15) and (21) in confined geometries (in fact, that is why we have considered the nonuniform distributions). For simplicity, we consider a rectangular sample with the length that is much larger than the width $L \gg W$, as well as any correlation length in the system. In this case, all physical quantities depend only on the transversal coordinate y $(-W/2 < y < W/2)$. If no contacts are attached to the side edges of the sample, the quasiparticle flows have to vanish at the edges

$$j_\alpha^y(y = \pm W/2) = 0. \quad (24)$$

Combining the carrier densities (13) into the charge density, $\delta n = \delta n_e - \delta n_h$, and total quasiparticle density $\delta\rho = \delta n_e + \delta n_h$, and introducing the corresponding currents, $\boldsymbol{j} = \boldsymbol{j}_h - \boldsymbol{j}_e$ and $\boldsymbol{P} = \boldsymbol{j}_e + \boldsymbol{j}_h$, we may represent the macroscopic equations (15) and (21) in the form[84]

$$D\boldsymbol{\nabla}\delta\rho + \boldsymbol{P} - \boldsymbol{j}\times\boldsymbol{\omega}_c\tau = 0, \quad (25a)$$

$$D\boldsymbol{\nabla}\delta n + \boldsymbol{j} - e\boldsymbol{E}\rho_0\tau/m - \boldsymbol{P}\times\boldsymbol{\omega}_c\tau = 0, \quad (25b)$$

$$\operatorname{div}\boldsymbol{P} = -\delta\rho/\tau_R, \qquad \operatorname{div}\boldsymbol{j} = 0. \quad (25c)$$

Looking for solutions independent of the x coordinate and keeping in mind the hard-wall boundary conditions (24), we find

$$\boldsymbol{P} = P(y)\boldsymbol{e}_y, \qquad \boldsymbol{j} = j(y)\boldsymbol{e}_x, \qquad \delta n = 0.$$

Moreover, we note that the equations (25) preserve the direction of the applied electric field if choose it to be

$$\boldsymbol{E} = E_0\boldsymbol{e}_x.$$

Then we can use Eq. (25c) to exclude the quasiparticle density and simplify Eqs. (25a) and (25b) as

$$-D\tau_R\,\partial^2 P/\partial y^2 + P(y) + \omega_c\tau j(y) = 0, \quad (26a)$$

$$j(y) = j_0 + \omega_c\tau P(y), \quad (26b)$$

where $j_0 = e\tau\rho_0 E_0/m$ is the electric current in the absence of magnetic field.

The second-order differential equation (26a) with the hard-wall boundary conditions (24) admits the solution[84]

$$P(y) = j_0\frac{\omega_c\tau}{1 + \omega_c^2\tau^2}\left(\frac{\cosh(2y/\ell_R)}{\cosh(W/\ell_R)} - 1\right), \quad (27)$$

where the quasiparticle recombination length in magnetic field is

$$\ell_R = \ell_0/\sqrt{1 + \omega_c^2\tau^2}, \qquad \ell_0 = 2\sqrt{D\tau_R}.$$

The quasiparticle current (27) and the corresponding electric current $\boldsymbol{j}(y)$ are illustrated in Fig. 1. The nonuniform nature of the currents does not allow for establishing a meaningful resistivity in our system. Instead, we may define the sheet resistance[84]

$$R_\square = E_0/\overline{J}, \qquad \overline{J} = \frac{e}{W}\int\limits_{-W/2}^{W/2} j(y)dy. \quad (28)$$

The resulting value of $R_\square$ is given by

$$R_\square = \frac{m}{e^2\tau\rho_0}\frac{1 + \omega_c^2\tau^2}{1 + \omega_c^2\tau^2 F(W/\ell_R)}, \quad F(x) = \frac{\tanh(x)}{x}. \quad (29)$$

The sheet resistance (29) was previously obtained in Ref. 84 using a phenomenological approach. Depending on the sample width W, recombination length ℓ_0, and magnetic field, one may identify three types of asymptotic behavior[84]:

(i) in wide samples, $W \gg (\omega_c\tau)^2\ell_R$, the resistance (29) is a non-saturating, quadratic function of the B field[73]

$$R_\square = \frac{m}{e^2\tau\rho_0}\left(1 + \omega_c^2\tau^2\right). \quad (30a)$$

The resistance (30a) exhibits geometric enhancement that is a consequence of the compensated hall effect, where the Hall voltage is absent despite the tilt of the carrier trajectories.

(ii) in narrow samples, $W \ll \ell_R$, quasiparticle recombination is ineffective, all currents flow along the x-axis, and hence the geometric enhancement factor is absent

$$R_\square = \frac{m}{e^2\tau\rho_0}. \quad (30b)$$

(iii) samples of intermediate width, $\ell_R \ll W \ll \omega_c^2\tau^2\ell_R$, in classically strong magnetic fields, $\omega_c\tau \gg 1$, exhibit a linear behavior[84,98]

$$R_\square = \frac{m}{e^2\tau\rho_0}\frac{W}{\ell_R}, \quad (30c)$$

shown in Eq. (7) above (note that $\omega_c\tau = \mu B$).

The results of this section provide the microscopic justification to the phenomenological approach of Ref. 84. Similar results were previously obtained for monolayer graphene[98]. In the following sections we generalize our theory to the case of arbitrary quasiparticle spectrum and prove that LMR in classically strong fields is a generic feature of compensated, two-component systems.

2. Symmetric bands with arbitrary spectrum

In this section, we generalize our kinetic theory to the case of the arbitrary quasiparticle spectrum, $\varepsilon(\boldsymbol{p})$, and energy-dependent momentum relaxation time, $\tau(\varepsilon)$. For simplicity, we only consider rotationally invariant spectra, $\varepsilon(\boldsymbol{p}) = \varepsilon_p$, $p = |\boldsymbol{p}|$. The cyclotron frequency is now also energy-dependent

$$\boldsymbol{\omega}_h = -\boldsymbol{\omega}_e = \boldsymbol{\omega}_c, \qquad \boldsymbol{\omega}_{\boldsymbol{c}}(\varepsilon) = e\boldsymbol{B}\,v/p, \qquad (31)$$

while the velocity and momentum are given by the usual relations

$$v(\varepsilon) = \left|\frac{\partial \varepsilon_p}{\partial p}\right|, \quad p = p(\varepsilon), \quad \varepsilon_{p(\varepsilon)} = \varepsilon. \qquad (32)$$

The energy dependence of the velocity and momentum relaxation time makes the derivation of the macroscopic transport equations rather tedious. Instead, we use the kinetic equation (8) to relate the two parts of the distribution function (17). The anisotropic part of the kinetic equation reads

$$\boldsymbol{v}\boldsymbol{\nabla} f_\alpha^{(i)} + e_\alpha \boldsymbol{E}\boldsymbol{v}\frac{\partial f_\alpha^{(i)}}{\partial \varepsilon} + \omega_\alpha(\varepsilon)\frac{\partial f_\alpha^{(a)}}{\partial \varphi} = -\frac{f_\alpha^{(a)}}{\tau(\varepsilon)}, \qquad (33)$$

where the angle φ describes direction of the velocity. Solving Eq. (33) for $f_\alpha^{(a)}$, we find

$$f_\alpha^{(a)} = \sum_{k,l} v^k \tau_\alpha^{kl} \left(-\frac{\partial}{\partial x^l} + e_\alpha E^l \frac{\partial}{\partial \varepsilon}\right) f_\alpha^{(i)}, \qquad (34)$$

where the indices $k, l = x, y$ indicate the 2D vector components. The tensor τ_α^{kl} is given by

$$\hat{\tau}_\alpha = \frac{\tau(\epsilon)}{1 + \omega_c^2(\varepsilon)\tau^2(\varepsilon)}\begin{pmatrix} 1 & \omega_\alpha(\varepsilon)\tau(\varepsilon) \\ -\omega_\alpha(\varepsilon)\tau(\varepsilon) & 1 \end{pmatrix}. \qquad (35)$$

Now we can use Eq. (33) to express the carrier flow densities (14) in terms of the isotropic part of the distribution function. Instead of the direct momentum integration, we now evaluate the currents (14) in two steps. Firstly, we average over the direction of the velocity. This yields the energy-dependent currents

$$j_\alpha^k(\varepsilon) = D_\alpha^{kl}(\varepsilon, B)\left(-\nabla^l + e_\alpha E^l \frac{\partial}{\partial \varepsilon}\right) f_\alpha^{(i)}, \qquad (36)$$

where $\hat{D}_\alpha(\varepsilon, B) = v^2 \hat{\tau}_\alpha/2$. Secondly, we integrate over the energy using the explicit form (18) of the distribution function. The expression (18) is still valid, since none of the assumptions of the previous section relied on the particular shape of the quasiparticle spectrum. Substituting Eq. (18) into Eq. (36) we find

$$j_\alpha^k(\varepsilon) = D_\alpha^{kl}(\varepsilon, B)\left[\nabla^l \delta\mu_\alpha(\boldsymbol{r}) + e_\alpha E^l\right]\frac{\partial f^{(0)}}{\partial \varepsilon}. \qquad (37)$$

Integrating Eq. (37) over the energy, we obtain

$$j_\alpha^k = D_\alpha^{kl}(B)\left(-\nabla^l \delta n_\alpha + e_\alpha \nu_0 E^l\right), \qquad (38)$$

with the averaged "diffusion tensor" is

$$\hat{D}_{e(h)}(B) = \frac{1}{\nu_0}\langle \hat{D}_\alpha(\varepsilon, B)\rangle = \begin{pmatrix} D_{xx} & \pm D_{xy} \\ \mp D_{xy} & D_{xx} \end{pmatrix}. \qquad (39a)$$

The individual matrix elements of $\hat{D}_{e(h)}(B)$ are given by

$$D_{xx} = \frac{1}{\nu_0}\left\langle \frac{v^2}{2}\frac{\tau(\varepsilon)}{1 + \omega_c^2(\varepsilon)\tau^2(\varepsilon)}\right\rangle, \qquad (39b)$$

$$D_{xy} = \frac{1}{\nu_0}\left\langle \frac{v^2}{2}\frac{\omega_c(\varepsilon)\tau^2(\varepsilon)}{1 + \omega_c^2(\varepsilon)\tau^2(\varepsilon)}\right\rangle. \qquad (39c)$$

For the energy-independent τ and ω_c the matrix $\hat{D}_{e(h)}(B)$ simplifies to

$$\hat{D}_\alpha(B) = \frac{D}{1 + \omega_c^2\tau^2}\begin{pmatrix} 1 & \omega_\alpha\tau \\ -\omega_\alpha\tau & 1 \end{pmatrix}, \qquad (40)$$

where D is given by Eq. (23).

The expression (38) generalizes the above macroscopic equation (21) for the case of an arbitrary quasiparticle spectrum and energy-dependent momentum relaxation rate [for the parabolic spectrum, we recover Eq. (21) with the help of the identity $\langle v^2/2\rangle = n_0/m$]. The corresponding continuity equations are still given by Eq. (15), where τ_R now stands for the mean value of the recombination time. Again, in this paper we do not study microscopic details of the recombination processes and, in particular, the energy dependence of the recombination rate.

At charge neutrality, the densities of electrons and holes coincide, $\delta n_h = \delta n_e = \delta\rho/2$. Similarly to the case of the parabolic spectrum, the hard-wall boundary conditions (24) ensure that the electric field does not deviate from its direction along the the x-axis, $\boldsymbol{E} = E_0\boldsymbol{e}_x$. This allows us to re-write Eq. (38) in the form

$$j_h^x = -j_e^x = e\nu_0 D_{xx}E_0 + \frac{1}{2}D_{xy}\frac{\partial\delta\rho}{\partial y}, \qquad (41a)$$

$$j_h^y = j_e^y = e\nu_0 D_{xy}E_0 - \frac{1}{2}D_{xx}\frac{\partial\delta\rho}{\partial y}. \qquad (41b)$$

Combining the currents (41) with the continuity equation (15), we find a second-order differential equation for $\delta\rho$

$$\frac{\partial^2\delta\rho}{\partial y^2} = \frac{4\delta\rho}{\ell_R^2}, \qquad \ell_R = 2\sqrt{D_{xx}\tau_R}. \qquad (42)$$

The equations (41) and (42) are completely equivalent to Eqs. (26). The only difference is the precise definition of the diffusion coefficients. Hence, it is not surprising that the solution to Eq. (42) with the hard-wall boundary conditions (24) is similar to Eq. (27)

$$\delta\rho = -e\nu_0 E_0 \ell_R \frac{D_{xy}}{D_{xx}}\frac{\sinh(2y/\ell_R)}{\cosh(W/\ell_R)}. \qquad (43)$$

Finally, we use the solution (43) and Eqs. (41) to find the averaged electric current and sheet resistance (28)

$$R_\square = \frac{1}{2e^2}\left(D_{xx} + \frac{D_{xy}^2}{D_{xx}}F(W/\ell_R)\right)^{-1}. \quad (44)$$

Qualitatively, the result (44) is similar to Eq. (29), see also Fig. 4. Most importantly, the dependence of $R_\square$ on the magnetic field and sample geometry is given by the same function $F(W/\ell_R)$. Therefore, we can identify the same three types of behavior as in Eqs. (30).

(i) in the limit of a *wide sample* the contribution of the function $F(W/\ell_R)$ may be neglected. The resulting magnetoresistance is quadratic and unsaturating, $R_\square \sim 1/D_{xx}$.

(ii) the limit of a *narrow sample* corresponds to the approximation $F(W/\ell_R) \approx 1$. In this case, the sheet resistance (44) is not strictly speaking a constant, but exhibits weak, quickly saturating dependence on the magnetic field, $R_\square \sim D_{xx}/(D_{xx}^2 + D_{xy}^2)$.

(iii) the limit of an *intermediate sample size* exists in classically strong magnetic fields, where we may approximate $F(x) \approx 1/x$ and neglect the field-independent term in Eq. (44). This leads to the linear magnetoresistance similar to Eq. (30c). The parameter range for this regime is similar to that of the previous section: $\ell_R \ll W \ll \ell_R D_{xy}^2/D_{xx}^2$. The resulting resistance is

$$R_\square = \frac{1}{2e^2}\frac{D_{xx}}{D_{xy}^2}\frac{W}{\ell_R}. \quad (45)$$

The result (45) may be simplified if we formally assume the limit $B \to \infty$. Then the elements of the diffusion matrix are

$$D_{xx} = \frac{\langle p^2/\tau\rangle}{2\nu_0 e^2 B^2}, \quad D_{xy} = \frac{\langle vp\rangle}{2\nu_0 eB}.$$

The recombination length is inverse proportional to the magnetic field

$$\ell_R = \frac{1}{eB}\sqrt{\frac{2\tau_R}{\nu_0}\left\langle\frac{p^2}{\tau}\right\rangle},$$

and hence the resistance is linear in the B-field

$$R_\square(B \to \infty) = \frac{B}{e}\sqrt{\frac{\nu_0\langle p^2/\tau\rangle}{2\tau_R}}\frac{\nu_0 W}{\langle vp\rangle^2}. \quad (46)$$

3. Asymmetric bands

Now we discuss a generic two-component system without electron-hole symmetry. For simplicity, we will consider the parabolic spectra (as we have seen above, changing the shape of the quasiparticle spectrum does not lead to qualitatively new physics)

$$\varepsilon_\alpha(\boldsymbol{p}) = \Delta/2 + p^2/2m_\alpha. \quad (47)$$

In addition, the system may be doped away from charge neutrality, i.e. the equilibrium chemical potential may be shifted from the middle of the band gap. Nevertheless, we may repeat the derivation of the continuity equations (15) and macroscopic equations (21) and arrive at the following description of the system

$$D_\alpha\boldsymbol{\nabla}\delta n_\alpha - e_\alpha\boldsymbol{E}n_{0,\alpha}\tau_\alpha/m_\alpha - \boldsymbol{j}_\alpha\times\boldsymbol{\omega}_\alpha\tau_\alpha = -\boldsymbol{j}_\alpha,$$

$$\operatorname{div}\boldsymbol{j}_\alpha = -(\Gamma_e\delta n_e + \Gamma_h\delta n_h)/2. \quad (48)$$

The electrons and holes are described by their respective densities $\delta n_\alpha(\boldsymbol{r}) = n_\alpha(\boldsymbol{r}) - n_{0,\alpha}$, masses m_α, momentum relaxation times τ_α, cyclotron frequencies $\boldsymbol{\omega}_\alpha = e_\alpha\boldsymbol{B}/m_\alpha c$, and diffusion coefficients

$$D_\alpha = \langle v^2\rangle_\alpha\tau_\alpha/(2\nu_{0,\alpha}). \quad (49)$$

Here the averaging over energies is similar to Eq. (20), but with the different equilibrium distribution functions for electrons and holes, $f_\alpha^{(0)}$:

$$\langle\cdots\rangle_\alpha = -\int\limits_{\Delta/2}^\infty d\varepsilon\,\nu_\alpha(\varepsilon)\frac{\partial f_\alpha^{(0)}}{\partial\varepsilon}(\cdots), \quad (50)$$

where $\nu_\alpha(\varepsilon)$ is the corresponding density of states.

The recombination rates Γ_α are generally different for electrons and holes and may be approximated as

$$\Gamma_e = 2\gamma n_{0,h}, \qquad \Gamma_h = 2\gamma n_{0,e}, \quad (51)$$

where the coefficient γ is the function of T and depends on a particular model of electron-hole recombination.

In the absence of the electron-hole symmetry, the classical Hall effect is no longer completely compensated and the Hall voltage is formed. The corresponding lateral component of the electric field can be related to the nonuniform charge density across the sample. In principle this can be done by solving the Poisson equation with the sample-specific boundary conditions. This electrostatic problem can be rather complicated and may admit only numerical solutions. While one may have to solve the electrostatic problem to describe the behavior of any particular sample quantitatively, qualitative physics is independent of such complications. Here, we will consider the simplest case of a gated sample. If the distance between the 2D electron system and the gate electrode is much smaller than any typical length scale describing inhomogeneity of the charge density and carrier flows, then the system is in the *strong screening* limit, where the electric field is related to the charge density as[84]

$$\boldsymbol{E} = E_0\boldsymbol{e}_x - \frac{e}{C}\frac{\partial\delta n}{\partial y}\boldsymbol{e}_y, \quad (52)$$

where E_0 is the external field, $C = \epsilon/4\pi d$ is the gate-to-channel capacitance per unit area, d is the the distance to the gate, ϵ is dielectric constant, and $\delta n = \delta n_h - \delta n_e$ is the charge density.

The macroscopic equations (48) are linear differential equations that can be solved similarly to the above case of the symmetric bands. Before presenting the general solution, we discuss two particular limiting cases, (i) the Boltzmann limit away from charge neutrality, and (ii) the fast Maxwell relaxation.

4. Boltzmann limit

First, we consider the low-temperature (Boltzmann) limit, $T \ll \Delta$, where the effective number of charge carriers in both bands is small. In the simplest case, the carriers have the same mass, $m_\alpha = m$, and momentum relaxation time, $\tau_\alpha = \tau = const$. Consequently, the two cyclotron frequencies also coincide, $\omega_h = -\omega_e = \omega_c$. The electron-hole symmetry is broken by the non-zero chemical potential, $\mu_{0,e} = -\mu_{0,h} = \mu$. The above parameters can be combined into the "Drude conductivities" of the electrons and holes

$$\sigma_{e(h)} = e^2 n_{0,e(h)} \tau / m. \tag{53}$$

In this limit, the equilibrium distribution functions have the simple form

$$f_{e(h)}^{(0)} = \exp\left(-\frac{\varepsilon + \Delta/2 \mp \mu}{T}\right), \tag{54}$$

allowing for the explicit expressions for the equilibrium carrier concentrations (with $\nu = gm/2\pi$ being the density of states for the 2D parabolic spectrum)

$$n_{0,e(h)} = \nu T \exp\left(-\frac{\Delta/2 \mp \mu}{T}\right). \tag{55}$$

Furthermore, with exponential accuracy the diffusion coefficients (49) can be approximated by

$$D_\alpha = D = T\tau/m. \tag{56}$$

The above simplifications allow for a straightforward solution of the macroscopic equations (48). The averaged sheet resistance (28) is given by

$$R_\square = \frac{1}{\sigma_e + \sigma_h} \frac{1 + \omega_c^2 \tau^2}{1 + \omega_c^2 \tau^2 \left[\xi + (1-\xi)F(W/\ell_R)\right]}, \tag{57}$$

where $\xi = n_0^2/\rho_0^2$ and the magnetic-field dependent recombination length ℓ_R is

$$\ell_R = 2\sqrt{\frac{2eD}{(\Gamma_e + \Gamma_h)(1 + \omega_c^2 \tau^2)}}. \tag{58}$$

At charge neutrality, $\xi = 0$, we recover the previous result (29). The magnetoresistance $R_\square(B)$ is shown in Fig. 3 for several values of ξ.

Since the system is doped away from charge neutrality, the classical Hall effect is no longer fully compensated.

This can be seen in the solution to the equations (48), where the electric field acquires a constant component in the lateral direction

$$E_y = -\frac{\omega_c \tau E_0 (\sigma_e - \sigma_h)}{\sigma_h + \sigma_e + DC}, \tag{59}$$

leading to the nonzero Hall voltage, $V_H = E_y W$. The corresponding Hall sheet resistance

$$R_\square^H = E_y/\overline{J} = R_\square E_y/E_0,$$

is given by

$$R_\square^H = -\frac{\omega_c \tau}{\sigma_e + \sigma_h + DC} \frac{\sigma_e - \sigma_h}{\sigma_e + \sigma_h} \tag{60}$$

$$\times \frac{1 + \omega_c^2 \tau^2}{1 + \omega_c^2 \tau^2 \left[\xi + (1-\xi)F(W/\ell_R)\right]}.$$

5. Fast Maxwell relaxation

A more general situation with unequal carrier masses and momentum relaxation times also allows for a simple solution under the assumption of fast Maxwell relaxation,

$$C \ll m_\alpha e^2.$$

In this limit, charge fluctuations in the two-component system relax much faster than the usual diffusion.

Formally taking the limit $C \to 0$ in Eqs. (48) and (52), we recover the balance between the nonequilibrium density fluctuations of the electrons and holes

$$\delta n_e = \delta n_h = \delta \rho/2. \tag{61}$$

Note, that this does not imply charge neutrality, since these fluctuations occur on the background of nonzero equilibrium charge density n_0.

Now, we can express the quasiparticle flows (14) in terms of the density perturbation (61) and electric field

$$j_\alpha^k = \left(\frac{e_\alpha E^l n_{0,\alpha} \tau_\alpha}{m_\alpha} - \frac{D_\alpha \nabla^l \delta\rho}{2}\right) \tau^{lk}, \tag{62}$$

where

$$\hat{\tau} = \frac{1}{1 + \omega_\alpha^2 \tau_\alpha^2} \begin{pmatrix} 1 & \omega_\alpha \tau_\alpha \\ -\omega_\alpha \tau_\alpha & 1 \end{pmatrix}. \tag{63}$$

Here the cyclotron frequency, $\omega_\alpha = e_\alpha B/m_\alpha$, has the opposite sign for electrons and holes.

The hard-wall boundary conditions (24) imply the equality $j_e^y = j_h^y$. Excluding the y-component of the electric field from Eqs. (62), we can express the currents j_α^y in terms of the quasiparticle density $\delta\rho$. This allows us to rewrite the continuity equations in the form of the second-order differential equation on $\delta\rho(y)$, same as Eq. (42), which we reproduce here for convenience,

$$\frac{d^2 \delta\rho}{dy^2} = \frac{4\delta\rho}{\ell_R^2}. \tag{64}$$

In contrast to Eq. (42), the effective recombination length is now given by

$$\ell_R = 2\sqrt{\frac{\sigma_e^{xx}D_h^{xx} + \sigma_h^{xx}D_e^{xx}}{(\Gamma_e + \Gamma_h)(\sigma_e^{xx} + \sigma_h^{xx})}}, \qquad (65)$$

where the two-component quasiparticle system is characterized by the field-dependent conductivity matrix

$$\hat{\sigma}_\alpha = \begin{pmatrix} \sigma_\alpha^{xx} & \sigma_\alpha^{xy} \\ \sigma_\alpha^{yx} & \sigma_\alpha^{xx} \end{pmatrix} = \frac{e^2 n_\alpha^0 \tau_\alpha}{m_\alpha}\hat{\tau}, \qquad (66a)$$

and the field-dependent diffusion matrix

$$\hat{D}_\alpha(B) = \begin{pmatrix} D_\alpha^{xx} & D_\alpha^{xy} \\ D_\alpha^{yx} & D_\alpha^{xx} \end{pmatrix} = D_\alpha \hat{\tau}. \qquad (66b)$$

The solution to Eq. (64), which satisfies the boundary conditions, differs from the previous result (43) by the normalization factor that is dictated by the relation (62) between the density and quasiparticle flows. In the present case we find

$$\delta\rho = -E_0 \ell_R \frac{\sigma_e^{xx}|\sigma_h^{xy}| + |\sigma_e^{xy}|\sigma_h^{xx}}{\sigma_e^{xx}D_h^{xx} + \sigma_h^{xx}D_e^{xx}} \frac{\sinh(2y/\ell_R)}{\cosh(W/\ell_R)}. \qquad (67)$$

Substituting Eq. (67) into Eq. (62), we express the inverse sheet resistance in the form

$$R_\square^{-1} = (\rho_\infty^{xx})^{-1} + AF(W/\ell_R), \qquad (68)$$

where ρ_∞^{xx} is the resistivity of an infinitely large system

$$\hat{\rho}_\infty = (\hat{\sigma}_e + \hat{\sigma}_h)^{-1}. \qquad (69)$$

and

$$A = \frac{(\sigma_e^{xx}|\sigma_h^{xy}| + |\sigma_e^{xy}|\sigma_h^{xx})^2}{(\sigma_e^{xx} + \sigma_h^{xx})\sigma_e^{xx}\sigma_h^{xx}}. \qquad (70)$$

The result (68), as well as the result of the previous section, Eq. (57), has the same functional dependence on the magnetic field as our previous result, Eq. (44). Therefore, also in the present case we can identify the three limiting cases of the wide, narrow, and intermediate-sized samples. In the latter case, we recover the linear dependence on the magnetic field. However, in contrast to the case of the neutral system, described by Eq. (44), the system away from charge neutrality exhibits saturation of the linear behavior. For illustration, we consider the formal limit $B \to \infty$, where the resistance (68) simplifies to

$$R_\square = \frac{m}{e^2 \rho_0 \tau} \frac{1}{\ell_R/W + n_0^2/\rho_0^2}. \qquad (71)$$

The linear behavior follows from the inverse proportionality of the recombination length to the magnetic field, $\ell_R \propto 1/B$. The saturation occurs when the field becomes so strong, that the ratio W/ℓ_R becomes comparable with ρ_0^2/n_0^2. Clearly, at charge neutrality $n_0 = 0$ and we recover the unsaturating behavior of Eq. (46).

6. General solution

Having discussed the limiting cases that allow for relatively simple and physically transparent solutions, we now turn to the most general case where the two quasiparticle subsystems are characterized by unrelated masses, momentum relaxation times, equilibrium densities, and recombination rates. We restrict ourselves to samples with rectangular geometry and again consider parabolic quasiparticle spectra (47), arguing that further generalization to arbitrary spectra will yield no additional physical insight. The main qualitative conclusion of this section is the same as before: in classically strong magnetic fields, there exists an intermediate parameter range, $\ell_0/\mu B \ll W \ll \ell_0 \mu B$ (here μ the some averaged mobility of electrons and holes), where the system exhibits linear magnetoresistance that is non-saturating at charge neutrality and saturates if the system is doped away from the neutrality point.

The general solution is most easily obtained upon re-writing the macroscopic equations (48) in the form similar to Eqs. (25), i.e. in terms of the total quasiparticle density $\delta\rho = \delta n_e + \delta n_h$, charge density fluctuations $\delta n = \delta n_e - \delta n_h$, quasiparticle flow $\boldsymbol{P} = \boldsymbol{j}_e + \boldsymbol{j}_h$, and electric current $\boldsymbol{j} = \boldsymbol{j}_h - \boldsymbol{j}_e$. Imposing the hard-wall boundary conditions (24) on the continuity equation for the electric current (25c), we find that the lateral component of $\boldsymbol{j}$ is equal to zero. All other quantities are functions of the lateral coordinate y. In particular, the macroscopic currents can be written as

$$\boldsymbol{j} = (j(y), 0), \qquad \boldsymbol{P} = (P_x(y), P_y(y)). \qquad (72)$$

The first of the equations (48) represents two vector equations. Re-writing them in terms of the currents $\boldsymbol{j}$ and $\boldsymbol{P}$ and writing the resulting equations in components, we obtain the following four equations

$$j = \sigma_+ E_0 + \omega_+ P_y, \qquad (73a)$$

$$P_x = \sigma_- E_0 + \omega_- P_y, \qquad (73b)$$

$$(D_+ + \kappa\sigma_+)\frac{\partial \delta n}{\partial y} + D_-\frac{\partial \delta\rho}{\partial y} + \omega_+ P_x + \omega_- j = 0, \quad (73c)$$

$$(D_- + \kappa\sigma_-)\frac{\partial \delta n}{\partial y} + D_+\frac{\partial \delta\rho}{\partial y} + \omega_- P_x + \omega_+ j = 0. \quad (73d)$$

Here we have used the short-hand notations

$$\sigma_\pm = e n_{0,e}\tau_e/m_e \pm e n_{0,h}\tau_h/m_h, \quad \omega_\pm = (\omega_e\tau_e \pm \omega_h\tau_h)/2,$$

$$D_\pm = (D_e \pm D_h)/2, \quad \kappa = e/C,$$

and took advantage of the gated electrostatics (52) in order to exclude the lateral component E_y.

The second of the equations (48) can be used to obtain the continuity equation relating the total quasiparticle density $\delta\rho$ and flow $\boldsymbol{P}$, generalizing Eq. (25c). The result can be represented in the form

$$\delta\rho = -\frac{1}{\gamma_+}\frac{\partial P_y}{\partial y} - \frac{\gamma_-}{\gamma_+}\delta n, \qquad (74)$$

where

$$\gamma_\pm = (\Gamma_e \pm \Gamma_h)/4.$$

Solution of the resulting system of equations (73), and (74) is straightforward, although tedious. Similarly to the above solutions of the particular limiting cases, we reduce the equations (73), and (74) to a single second-order differential equation, cf. Eqs. (26) and (42). Here it is convenient to reduce the problem to a second-order differential equation for P_y,

$$\frac{\partial^2 P_y}{\partial^2 y} = \frac{4}{\ell_R^2}P_y + \frac{s_0\gamma_- + s_1\gamma_+}{D_0^2}E_0, \qquad (75)$$

where the effective recombination length is given by

$$\ell_R = \frac{2D_0}{\sqrt{b_0\gamma_- + b_1\gamma_+}}, \qquad (76)$$

and the following notations are introduced

$$s_0 = (\sigma_+\omega_- + \sigma_-\omega_+)D_+ - (\sigma_+\omega_+ + \sigma_-\omega_-)D_-,$$

$$s_1 = (\sigma_+\omega_+ + \sigma_-\omega_-)(D_+ + \kappa\sigma_+) - (\sigma_+\omega_- + \sigma_-\omega_+)(D_- + \kappa\sigma_-),$$

$$D_0 = \sqrt{D_+(D_+ + \kappa\sigma_+) - D_-(D_- + \kappa\sigma_-)},$$

$$b_0 = 2\omega_+\omega_-D_+ - (1 + \omega_+^2 + \omega_-^2)D_-,$$

$$b_1 = (1 + \omega_+^2 + \omega_-^2)(D_+ + \kappa\sigma_+) - 2\omega_+\omega_-(D_- + \kappa\sigma_-).$$

Solving the differential equation (75) with the hard-wall boundary conditions $P_y(\pm W/2) = 0$ [cf. Eq. (24)], we average the result over the y coordinate [cf. Eq. (28)],

$$\overline{P_y} \equiv \frac{1}{W}\int_{-W/2}^{W/2} dy\, P_y(y), \qquad (77)$$

and obtain the solution

$$\overline{P_y} = E_0\frac{s_0\gamma_- + s_1\gamma_+}{b_0\gamma_- + b_1\gamma_+}\left[F(W/\ell_R) - 1\right]. \qquad (78)$$

Again, we have used the notation $F(x) = \tanh(x)/x$.

Finally, we average the relation (73a) in order to find the average electric current, $\overline{J} = -e\overline{j}$, and use the definition (28) in order to find the inverse sheet resistance

$$R_\square^{-1} = e\left[\sigma_+ + \omega_+\left[F(W/\ell_R) - 1\right]\frac{s_0\gamma_- + s_1\gamma_+}{b_0\gamma_- + b_1\gamma_+}\right]. \qquad (79)$$
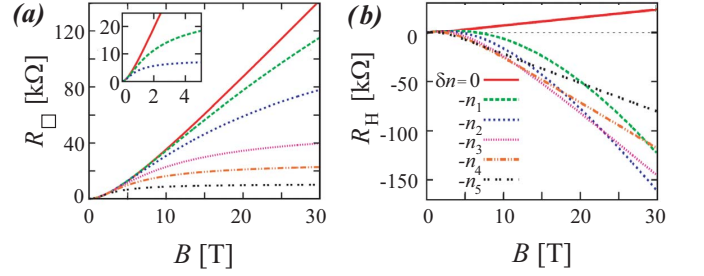

FIG. 4: The magnetic field dependence of the sheet longitudinal (left) and Hall resistance (right) given by Eqs. (79) and (80). The numerical values were obtained using the typical experimental parameters of topological-insulator films: electron and hole mobilities $\mu_e = 20\mu_h$, $\mu_h = 1$ m^2/(V·s) and velocities $v_e = 10^6$ m/s, $v_h = 0.5 v_e$, and the sample parameters are $W = 10\mu$m, $d = 0.5\mu$m, and $\epsilon = 5$. The carrier densities were calculated using a generic two-band model with the energy gap $\Delta = 4$ meV at room temperature $T = 300$ K. The recombination length in the absence of magnetic field at charge neutrality is $\ell_0 = 0.37\mu$m. The solid line corresponds to charge neutrality, $\delta n = 0$, while the other lines correspond to negative densities $\delta n = 0.3, 0.5, 0.9, 1.3, 2.1 \times 10^{11}$ cm^{-2}. The inset in the left panel shows the magnetoresistance $R_\square$ for a symmetric model with $\mu_\alpha = 20$ m^2/(V·s).

Averaging the y-component of the electric field [cf. Eq. (52)], we find

$$\overline{E_y} = -\kappa\overline{\frac{\partial\delta n}{\partial y}} = \kappa\frac{s_0 E_0 + b_0\overline{P_y}}{D_0^2} = \eta\, E_0,$$

with

$$\eta = \frac{\kappa}{D_0^2}\left[s_0 + b_0\left[F(W/\ell_R) - 1\right]\frac{s_0\gamma_- + s_1\gamma_+}{b_0\gamma_- + b_1\gamma_+}\right].$$

As a result, the Hall resistance of the sheet is given by

$$R_\square^H = \overline{E_y}/\overline{J} = \eta\, R_\square. \qquad (80)$$

The results of Eqs. (79) and (80) are shown in Fig. 4, where we plot our results using realistic parameters for topological-insulator films.

The field dependence of the resistance (79) comes from the recombination length (76) as well as from the explicit dependence on the parameters s_i and b_i. However, for classically strong fields, $\omega_\pm \gg 1$, the latter dependence cancels out since in this limit the quantities s_i are proportional to the magnitude of the field, $s_i = S_i B$, while b_i are proportional to the square of the field, $b_i = B_i B^2$. The proportionality coefficients

$$S_0 = (\sigma_+\mu_- + \sigma_-\mu_+)D_+ - (\sigma_+\mu_+ + \sigma_-\mu_-)D_-,$$

$$S_1 = (\sigma_+\mu_+ + \sigma_-\mu_-)(D_+ + \kappa\sigma_+) - (\sigma_+\mu_- + \sigma_-\mu_+)(D_- + \kappa\sigma_-),$$

$$B_0 = 2\mu_+\mu_-D_+ - (\mu_+^2 + \mu_-^2)D_-,$$

$$B_1 = \left(\mu_+^2 + \mu_-^2\right)(D_+ + \kappa\sigma_+) - 2\mu_+\mu_-(D_- + \kappa\sigma_-),$$

are expressed in terms of the effective mobilities

$$\mu_\pm = \frac{e}{2c}\left(\frac{\tau_e}{m_e} \pm \frac{\tau_h}{m_h}\right).$$

Then the resistance (79) becomes similar to all of the above results (29), (44), (57), and (68), insofar the field dependence is confined to the recombination length ℓ_R in the argument of the function $F(W/\ell_R)$. Hence, also the general solution exhibits the three parameter regimes of a "wide", "narrow", and "intermediate-sized" sample. In the most interesting latter case, the dependence of the resistance (79) on the magnetic field may be illustrated by considering the formal limit $B \to \infty$. Then the result can be expressed in the following simple form,

$$R_\square^{-1} = e\left[\sigma_0 + \frac{M}{B}\right], \tag{81}$$

where

$$\sigma_0 = \sigma_+ - \frac{\mu_+(S_0\gamma_- + S_1\gamma_+)}{B_0\gamma_- + B_1\gamma_+}, \tag{82a}$$

$$M = \frac{2D_0\sigma_+(S_0\gamma_- + S_1\gamma_+)}{W(B_0\gamma_- + B_1\gamma_+)^{3/2}}. \tag{82b}$$

At the neutrality point, where $n_{0,e} = n_{0,h} = \rho_0/2$, the parameters of the solution simplify as $\sigma_\pm = \rho_0\mu_\pm/2$, and thence $S_{0(1)} = \rho_0 B_{0(1)}/2$. As a result, $\sigma_0 = 0$, and we recover the non-saturating LMR.

The results of the previous sections can be obtained from Eqs. (79) and (81) by taking the appropriate limits. For example, close to charge neutrality, the quantity σ_0 is determined by the equilibrium charge density both in the cases of the electron-hole symmetry and fast Maxwell relaxation ($\kappa \to \infty$). In the limit $n_0 \to 0$, we find $\sigma_0 \propto n_0^2$ and hence

$$R_\square^{-1} = \sigma_+\left(\xi + \ell_R/W\right), \tag{83}$$

where $\xi = n_0^2/\rho_0^2$, similar to Eqs. (57) and (71).

B. Hydrodynamic approach

When the shortest time scale in the problem is due to electron-electron interaction,

$$\tau_{ee}^{-1} \gg \tau_{imp}^{-1}, \ \tau_{ph}^{-1}, \tag{84}$$

electronic transport may be described using the universal hydrodynamic approach.

The standard derivation of the hydrodynamic equations relies on the assumption of local equilibrium, which in a two-component system could be described by the distribution function

$$f_\alpha = \frac{1}{\exp\left\{\left[\varepsilon_\alpha(\boldsymbol{p}) - \boldsymbol{p}\boldsymbol{u}_\alpha(\boldsymbol{r}) - \mu_\alpha(\boldsymbol{r})\right]/T(\boldsymbol{r})\right\} + 1}. \tag{85}$$

The electronic fluid is characterized by the local temperature $T(\boldsymbol{r})$, chemical potentials $\mu_\alpha(\boldsymbol{r})$, and drift velocities $\boldsymbol{u}_\alpha(\boldsymbol{r})$. This distribution function nullifies the electron-electron and hole-hole collision integrals, but not the electron-hole collision integral. This means that the standard approach can only be used if the coupling between the two types of charge carriers is relatively weak. This is what happens, for example, in double-layer systems[91], where the two types of carriers belong to physically different layers of the sample.

A complete analytic solution of the kinetic equation of a generic two-component system with an arbitrary spectrum is not known. The problem can be solved in a Fermi liquid[96], but the resulting theory is rather cumbersome. At the same time, the final form of the hydrodynamic equations, especially within linear response[98], is universal and is typically believed to be applicable to most experimentally accessible systems. Here we consider an electron-hole symmetric $[\varepsilon_\alpha(\boldsymbol{p}) = \varepsilon_{\boldsymbol{p}}]$ system at charge neutrality under a model assumption

$$\tau_{eh}^{-1} \ll \tau_{hh}^{-1} = \tau_{ee}^{-1}. \tag{86}$$

In this case, the equilibration within each subsystem is much faster than their mutual scattering, so that we can use the distribution function (85) as a starting point. Furthermore, we expect that even if $\tau_{eh} \sim \tau_{hh} \sim \tau_{ee}$ the effective hydrodynamic description remains valid and describes the physics of the system at least qualitatively. Remarkably, in graphene[97–104] one can rigorously show that the hydrodynamic approach yields a good quantitative description of electronic transport despite the fact that the inequality (86) is violated.

For simplicity, we will assume the parabolic spectrum and energy-independent impurity scattering time. Generalization to a more general situation is straightforward.

Within linear response, the distribution function (85) may be expanded as

$$f^\alpha = f^{(0)} + \delta f^\alpha, \tag{87}$$

$$\delta f^\alpha = -\frac{\partial f^{(0)}}{\partial\varepsilon}\left(\delta\mu_\alpha + \varepsilon_{\boldsymbol{p}}\frac{\delta T}{T} + \boldsymbol{p}\,\boldsymbol{u}_\alpha\right), \tag{88}$$

where $\delta\mu_\alpha$, δT, and $\boldsymbol{u}_\alpha$ are proportional to the electric field $\boldsymbol{E}$.

Similarly to the disorder-dominated regime discussed in Sec II A, we assume here that thermalization between the electronic system and the lattice is much faster than quasiparticle recombination (even though both processes are ultimately due to electron-phonon scattering)

$$\tau_{ph} \ll \tau_R.$$

This allows us to neglect local temperature fluctuations

$$\delta T(\boldsymbol{r}) = 0.$$

In this case, electrons and hole densities are related to fluctuations of the chemical potential, $\delta\mu_\alpha$, by means of

Eq. (19), while the currents are proportional to hydrodynamic velocities

$$\boldsymbol{j}_\alpha = m\langle v^2\rangle\boldsymbol{u}_\alpha/2 = \langle\varepsilon - \Delta/2\rangle\boldsymbol{u}_\alpha. \tag{89}$$

We remind the reader, that the averaging over all single-particle states within a given band as defined in Eq. (20) is not dimensionless. The resulting averaged quantity has dimensions of the original quantity divided by an extra dimension of energy, such that the expression $\langle\varepsilon\rangle$ is dimensionless.

Usually, the hydrodynamic equations are derived by multiplying the kinetic equation (8) by symmetry-related factors and integrating over all single-particle states. In particular, integrating the kinetic equation itself (i.e. with the factor of unity) yields the continuity equations manifesting the particle number conservation. In two-component systems, the continuity equations (15) contain extra factors reflecting quasiparticle recombination. Integration of the kinetic equation multiplied by the quasiparticle velocities leads to the macroscopic equations for the quasiparticle current flows

$$D\boldsymbol{\nabla}\delta n_h - e\boldsymbol{E}\rho_0\tau/(2m) - \boldsymbol{j}_h\times\boldsymbol{\omega_c}\tau - \boldsymbol{F}_{eh} = -\boldsymbol{j}_h, \tag{90a}$$

$$D\boldsymbol{\nabla}\delta n_e + e\boldsymbol{E}\rho_0\tau/(2m) + \boldsymbol{j}_e\times\boldsymbol{\omega_c}\tau + \boldsymbol{F}_{eh} = -\boldsymbol{j}_e, \tag{90b}$$

which differ from Eq. (21) only by the presence of the friction force

$$\boldsymbol{F}_{eh} = \chi(\boldsymbol{j}_e - \boldsymbol{j}_h)/2, \tag{91}$$

where $\chi\simeq\tau/\tau_{\rm eh}$. Under our assumption (86), the parameter χ is necessarily small, even though in the hydrodynamic regime $\tau/\tau_{\rm ee}\gg 1$ and $\tau/\tau_{\rm hh}\gg 1$.

At charge neutrality, the currents and densities for the two quasiparticle branches are not independent for the electron-hole symmetry dictates the following relations: $\delta n_h = \delta n_e = \delta\rho/2$, $j_e^x = -j_h^x = j/2$, and $j_e^y = j_h^y = P/2$. Hence, the continuity equations (15) and macroscopic equations (90) may be re-written in the form

$$eE\rho_0\tau/m - (1+\chi)j + \omega_c\tau P = 0, \tag{92a}$$

$$D\partial\delta\rho/\partial y + P + \omega_c\tau j = 0, \tag{92b}$$

$$\partial P/\partial y = -\delta\rho/\tau_R, \tag{92c}$$

Solving the above equations with the hard-wall boundary conditions (24), which imply $P(\pm W/2) = 0$, we find

$$\delta\rho = -\frac{eE_0\ell_R\rho_0\tau}{4m}\frac{\omega_c\tau}{D(1+\chi)}\frac{\sinh(2y/\ell_R)}{\cosh(W/\ell_R)}, \tag{93a}$$

$$R_\square == \frac{m(1+\chi)}{e^2\rho_0\tau}\frac{1+\chi+\omega_c^2\tau^2}{1+\chi+\omega_c^2\tau^2 F(W/\ell_R)}, \tag{93b}$$

where the effective recombination length is given by

$$\ell_R = 2\sqrt{\frac{(1+\chi)D\tau_R}{1+\chi+\omega_c^2\tau^2}}. \tag{94}$$

The dependence of the resistance (93b) on the magnetic field is once again controlled by the function $F(W/\ell_R)$. Similarly to the above discussion of the general disorder-dominated sample, we illustrate the behavior of the resistance in the "intermediate-sized" sample in classically strong magnetic fields by formally taking the limit $B\to\infty$, which here means $\omega_c\tau\gg\sqrt{1+\chi}$ and $W\gg\ell_R$. In this case we again find the linear behavior

$$R_\square = \frac{\sqrt{1+\chi}}{2e\rho_0\sqrt{D\tau_R}}B. \tag{95}$$

The results of this section are qualitatively similar to those previously obtained in the disorder-dominated regime. In particular, the resistance (93b) differs from Eq. (29) by the presence of the parameter χ describing the mutual friction between the two carrier subsystems. The friction slightly modifies the equation for the electric current (92a) as compared to Eq. (25a), while the continuity equations and the equation for the total quasiparticle flow (92b) remain the same as Eqs. (25c) and (25b), respectively. This gives us confidence, that the equations (92) provide us with a general description of electronic transport in two-component systems close to charge neutrality. Even though the derivation carried out in this section relied on the simplified model assumption (86), the resulting equations (92) will remain valid for any value of the electron-hole scattering rate $1/\tau_{\rm eh}$.

III. TRANSPORT THEORY OF 3D TWO-COMPONENT SYSTEMS

Now we turn to the study of magnetoresistance in 3D two-component systems. Our goal is to demonstrate, that within the "classical" range of magnetic fields, the physics of the phenomenon remains the same as in the 2D case discussed above. However, practical calculations are in general difficult. The two main reasons for the difficulties are (i) the need to solve the 3D Poisson equation to account for the sample electrostatics, and (ii) a large number of parameter regimes characterized by competing length scales related to the sample geometry and microscopic details of the charge carriers, as well as possible spatial orientations of the applied magnetic field.

In this paper we try to avoid the technical complications as much as possible by considering a particular "rectangular" sample geometry, see Fig. 5. We consider a sample in the form of a "slab", which is "infinitely" long (i.e., much longer than any characteristic length scale in the problem) in one direction, that we refer to as x-direction, while the lateral cross-section of the sample has a form of a thin rectangle, with one side being much longer than another, $d\gg W$ (but still much shorter than the sample size in the x-direction). This particular shape of the sample allows us to assume that any transport-related quantity is a function of only one coordinate, y.

We assume that the external electric field is applied along the x-direction, $\boldsymbol{E} = E_0\boldsymbol{e}_x$. Consequently, the elec-
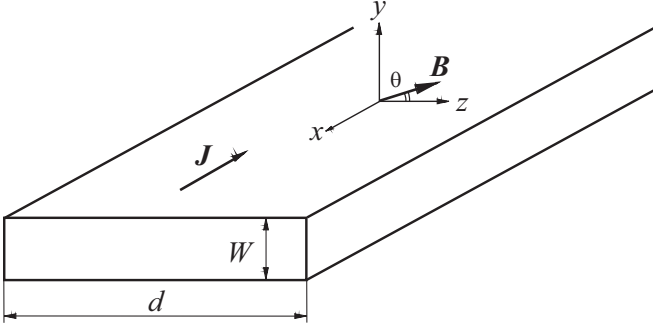
FIG. 5: 3D sample with the shape of a slab in an oblique magnetic field. The magnetic field vector lies in the xy plane.

tric current is also flowing in the x-direction (assuming the hard-wall boundary conditions in y and z directions)

$$\boldsymbol{j} = j(y)\boldsymbol{e}_x. \tag{96}$$

The applied magnetic field lies in the yz-plane,

$$\boldsymbol{B} = B\left(0,\ \sin\theta,\ \cos\theta\right). \tag{97}$$

In what follows, we will first consider a particularly simple case, where the magnetic field is directed along the z-axis ($\theta = 0$) and then discuss the problem with arbitrary θ, focusing on the neutrality point.

A. Magnetic field orthogonal to the thin, long face of the cuboid sample

Let us first consider the technically simpler situation where the magnetic field is applied along the z direction. In this case, the classical Hall voltage is generated across the y direction. The relation between the electric field and quasiparticle flows is given by the standard Ohm's law [cf. Eq. (38) in the 2D problem]

$$ej_h^y = \sigma_h^{xy}E_0 + \sigma_h^{xx}E_y - eD_h^{xx}\frac{d\delta n_h}{dy}, \tag{98a}$$

$$ej_e^y = \sigma_e^{xy}E_0 - \sigma_e^{xx}E_y - eD_e^{xx}\frac{d\delta n_e}{dy}, \tag{98b}$$

$$ej_h^x = \sigma_h^{xx}E_0 - \sigma_h^{xy}E_y + eD_h^{xy}\frac{d\delta n_h}{dy}, \tag{98c}$$

$$ej_e^x = -\sigma_e^{xx}E_0 - \sigma_e^{xy}E_y - eD_e^{xy}\frac{d\delta n_e}{dy}. \tag{98d}$$

In this section, we do not derive the elements of the conductivity tensor σ_α^{kl} and the diffusion constants D_α^{kl} from the microscopic theory, but rather treat them as

macroscopic (phenomenological) parameters of the system. Furthermore, we will assume the usual dependence of σ_α^{kl} and D_α^{kl} on the external magnetic field, see Eqs. (39) (40), and (66).

The quasiparticle flows, $j_{e(h)}^y$, obey the continuity equations

$$\frac{dj_h^y}{dy} = -(\Gamma_h\delta n_h + \Gamma_e\delta n_e), \tag{99a}$$

$$\frac{dj_e^y}{dy} = -(\Gamma_h\delta n_h + \Gamma_e\delta n_e), \tag{99b}$$

where $\Gamma_{e(h)}$ are the corresponding recombination rates.

Finally, the 3D Poisson equation yields the relationship between the electric field in the Hall direction and quasiparticle densities,

$$\frac{dE_y}{dy} = 4\pi e(\delta n_h - \delta n_e). \tag{100}$$

Combining the above equations (98), (99) and (100), we derive a closed system of second-order differential equations for the quasiparticle density fluctuations [cf. Eqs. (42) and (64)]

$$\frac{d^2}{dy^2}\begin{pmatrix}\delta n_h \\ \delta n_e\end{pmatrix} = \widehat{K}^2\begin{pmatrix}\delta n_h \\ \delta n_e\end{pmatrix}, \tag{101a}$$

where the 2×2 matrix $\widehat{K}$ is given by

$$\widehat{K}^2 = \begin{pmatrix} \dfrac{\Gamma_h + 4\pi\sigma_h^{xx}}{D_h^{xx}} & \dfrac{\Gamma_e - 4\pi\sigma_h^{xx}}{D_h^{xx}} \\[3mm] \dfrac{\Gamma_h - 4\pi\sigma_e^{xx}}{D_e^{xx}} & \dfrac{\Gamma_e + 4\pi\sigma_e^{xx}}{D_e^{xx}} \end{pmatrix}. \tag{101b}$$

The above differential equations are subject to the hard-wall boundary conditions [cf. Eq. (24)]

$$j_\alpha^y(y = \pm W/2) = 0. \tag{102a}$$

The boundary conditions (102a) have to be supplemented by the vanishing boundary conditions[2] for the transversal electric field E_y (see also Appendix)

$$E_y(y = \pm W/2) = 0. \tag{102b}$$

The differential equations (98) - (101) with the boundary conditions (102) allow for the formal solution

$$\begin{pmatrix}\delta n_h \\ \delta n_e\end{pmatrix} = \frac{E_0}{e}\sinh\widehat{K}y\left[\widehat{K}\cosh\frac{\widehat{K}W}{2}\right]^{-1}\begin{pmatrix}\sigma_h^{xy}/D_h^{xx} \\ \sigma_e^{xy}/D_e^{xx}\end{pmatrix}, \tag{103a}$$

$$E_y = 4\pi E_0 \begin{pmatrix} 1 & -1 \end{pmatrix} \widehat{K}^{-1} \left[\cosh \widehat{K} y \left[\cosh \frac{\widehat{K}W}{2} \right]^{-1} - 1 \right] \widehat{K}^{-1} \begin{pmatrix} \sigma_h^{xy}/D_h^{xx} \\ \sigma_e^{xy}/D_e^{xx} \end{pmatrix}, \tag{103b}$$

$$\begin{pmatrix} j_h^y \\ j_e^y \end{pmatrix} = -\frac{E_0}{e} \begin{pmatrix} \Gamma_h & \Gamma_e \\ \Gamma_h & \Gamma_e \end{pmatrix} \widehat{K}^{-1} \left[\cosh \widehat{K} y \left[\cosh \frac{\widehat{K}W}{2} \right]^{-1} - 1 \right] \widehat{K}^{-1} \begin{pmatrix} \sigma_h^{xy}/D_h^{xx} \\ \sigma_e^{xy}/D_e^{xx} \end{pmatrix}, \tag{103c}$$

while the longitudinal currents j_α^x can be found from Eqs. (98c) and (98d). The averaged electric current (28) is

$$\overline{J} = E_0 \left[\sigma_h^{xx} + \sigma_e^{xx} + \frac{(\sigma_h^{xy} - \sigma_e^{xy})^2}{\sigma_h^{xx} + \sigma_e^{xx}} \right] \tag{103d}$$

$$+ E_0 \left(D_h^{xy} - 4\pi(\sigma_h^{xy} - \sigma_e^{xy}) \quad D_e^{xy} + 4\pi(\sigma_h^{xy} - \sigma_e^{xy}) \right) \widehat{F}\left(\frac{\widehat{K}W}{2} \right) \begin{pmatrix} \sigma_h^{xy}/D_h^{xx} \\ \sigma_e^{xy}/D_e^{xx} \end{pmatrix},$$

where

$$\widehat{F}\left(\frac{\widehat{K}W}{2} \right) = \frac{2}{W} \widehat{K}^{-1} \sinh \frac{\widehat{K}W}{2} \left[\cosh \frac{\widehat{K}W}{2} \right]^{-1}.$$

In an infinitely wide sample ($W \to \infty$), the function $\widehat{F}$ vanishes, leaving the classical result, see the first line of Eq. (103d). This comprises the Drude conductivity in the absence of the magnetic field and the classical, quadratic magnetoconductivity.

The solutions (103) are somewhat tedious. Similarly to Eqs. (42) and (64), the matrix $\widehat{K}$ defines two characteristic length scales, given by its eigenvalues, $\kappa_{1(2)}$. To make the discussion physically transparent, we focus on the two limiting cases.

1. Fast Maxwell relaxation

In the limit of fast Maxwell relaxation, determined by the inequality (the so-called "good metal" condition)

$$4\pi \sigma_\alpha^{xx} \gg \Gamma_\alpha, \tag{104a}$$

one of the eigenvalues determines the effective recombination length [cf. Eq. (65)]

$$\kappa_1^2 = \frac{4}{\ell_R^2} = \frac{(\Gamma_h + \Gamma_e)(\sigma_h^{xx} + \sigma_e^{xx})}{\sigma_h^{xx} D_e^{xx} + \sigma_e^{xx} D_h^{xx}}, \tag{104b}$$

while the other is related to the Thomas-Fermi screening length

$$\kappa_2^2 = 4\varkappa^2 = 4\pi \left(\frac{\sigma_h^{xx}}{D_h^{xx}} + \frac{\sigma_e^{xx}}{D_e^{xx}} \right) = 4\pi e^2 \left(\frac{\partial n_h}{\partial \mu} + \frac{\partial n_e}{\partial \mu} \right). \tag{104c}$$

Here $\partial n_\alpha/\partial\mu = \sigma_\alpha^{xx}/(e^2 D_\alpha^{xx})$ is the thermodynamic density of states. In a typical situation, where the conductivities and diffusion coefficients for electrons and holes

are of the same order of magnitude, the condition for the fast Maxwell relaxation (104a) can be re-written in one of the two equivalent forms

$$\kappa_1 \ll \kappa_2, \qquad \varkappa \ell_R \gg 1. \tag{104d}$$

In classically strong magnetic fields, $\omega_\alpha \tau_\alpha \gg 1$, the recombination length is inverse proportional to the field,

$$\ell_R \sim 1/B, \tag{104e}$$

while the Thomas-Fermi screening length is approximately field-independent.

In the limit (104d), the results (103) simplify. Combining the densities (103a) into the charge and quasiparticle densities, we find near one of the boundaries ($y \approx W/2$)

$$e\delta n = \frac{E_0}{2\varkappa} \left[e^{-\varkappa(W-2y)} \left(\frac{\sigma_h^{xy}}{D_h^{xx}} - \frac{\sigma_e^{xy}}{D_e^{xx}} \right) \right. \tag{105a}$$

$$\left. - \frac{e^{-(W-2y)/\ell_R}}{\varkappa \ell_R} \frac{\sigma_e^{xy}\sigma_h^{xx} + \sigma_h^{xy}\sigma_e^{xx}}{\sigma_e^{xx} + \sigma_h^{xx}} \left(\frac{1}{D_h^{xx}} - \frac{1}{D_e^{xx}} \right) \right],$$

$$\delta\rho = \frac{E_0}{e} \left[e^{-\varkappa(W-2y)} \frac{D_e^{xx}\sigma_h^{xx} - D_h^{xx}\sigma_e^{xx}}{D_e^{xx}\sigma_h^{xx} + D_h^{xx}\sigma_e^{xx}} \left(\frac{\sigma_h^{xy}}{D_h^{xx}} - \frac{\sigma_e^{xy}}{D_e^{xx}} \right) \right.$$

$$\left. + \ell_R e^{(W-2y)/\ell_R} \frac{\sigma_e^{xx}\sigma_h^{xy} + \sigma_h^{xx}\sigma_e^{xy}}{D_e^{xx}\sigma_h^{xx} + D_h^{xx}\sigma_e^{xx}} \right]. \tag{105b}$$

The results (105) demonstrate the existence of *two* boundary layers forming in the two-component system: (i) the narrow (in the present limit of fast Maxwell relaxation) *screening layer*, see also Appendix, and (ii) the wide *recombination layer*. The latter is similar to the boundary layer found above in the 2D systems.

The spatial profile of the lateral electric field near the

boundary is similar to Eq. (105a)

$$E_y = E_0 \left[\frac{\sigma_e^{xy} - \sigma_h^{xy}}{\sigma_e^{xx} + \sigma_h^{xx}} + \frac{\pi}{\varkappa^2} e^{-\varkappa(W-2y)} \left(\frac{\sigma_h^{xy}}{D_h^{xx}} - \frac{\sigma_e^{xy}}{D_e^{xx}} \right) \right. \quad (106)$$

$$\left. - \frac{\pi}{\varkappa^2} e^{-(W-2y)/\ell_R} \frac{\sigma_e^{xy}\sigma_h^{xx} + \sigma_h^{xy}\sigma_e^{xx}}{\sigma_e^{xx} + \sigma_h^{xx}} \left(\frac{1}{D_h^{xx}} - \frac{1}{D_e^{xx}} \right) \right].$$

The two quantities satisfy the Poisson equation (100).

Finally, the second line in the averaged current (103d) yields the linear contribution to the magnetoconductivity, which we attribute to the surface regions of the sample [as opposed to the classical bulk contribution given by the first line in Eq. (103d)]

$$\overline{\sigma}_s \approx 2\frac{\ell_R}{W} \frac{(D_h^{xy} + D_e^{xy})(\sigma_e^{xx}\sigma_h^{xy} + \sigma_h^{xx}\sigma_e^{xy})}{D_h^{xx}\sigma_e^{xx} + D_e^{xx}\sigma_h^{xx}}. \quad (107)$$

Here we have assumed $\tanh \kappa_{1(2)}W \approx 1$, corresponding to the intermediate sample widths as discussed in the 2D case, and used Eq. (104d) to neglect the contribution of the second eigenvalue κ_2. The latter is quadratic in the magnetic field, but vanishes exactly in any compensated system, similarly to the classical magnetoresistance [as well as the lateral electric field (106) and the fluctuation of the charge density (105a)].

As a result, a 3D compensated system in orthogonal magnetic field exhibits linear magnetoresistance in the limit of fast Maxwell relaxation similarly to the 2D case.

2. Slow Maxwell relaxation

In very strong magnetic fields the condition (104a) for fast Maxwell relaxation is violated and the results (105), (106), and (107) become invalid. Assuming that the motion of charge carriers remains classical, one may consider the opposite limit of slow Maxwell relaxation where

$$4\pi\sigma_\alpha^{xx} \ll \Gamma_\alpha. \quad (108a)$$

In this case, the eigenvalues of the matrix $\widehat{K}$ (which again are labeled such that $\kappa_2 \gg \kappa_1$) are given by

$$\kappa_1^2 = 4\pi \frac{(\Gamma_h + \Gamma_e)(\sigma_h^{xx} + \sigma_e^{xx})}{\Gamma_h D_e^{xx} + \Gamma_e D_h^{xx}}, \quad (108b)$$

$$\kappa_2^2 = \Gamma_h/D_h^{xx} + \Gamma_e/D_e^{xx}. \quad (108c)$$

There are still two length scales characterizing the system. Assuming that the model parameters describing electrons and holes are of the same order of magnitude, we may associate the smaller eigenvalue κ_1 with the inverse Thomas-Fermi screening length and the larger eigenvalue κ_2 with the inverse recombination length:

$$\kappa_1 \sim \varkappa, \qquad \kappa_2 \sim 1/\ell_R, \qquad \varkappa\ell_R \ll 1.$$

Repeating the calculation leading to Eq. (107) one would now conclude that the dominant contribution to the magnetoconductivity is given by the much wider screening surface layer. However, this contribution

$$\overline{\sigma}_{sc} \approx \frac{2}{\kappa_1 W} \frac{\Gamma_h D_e^{xy} - \Gamma_e D_h^{xy} + 4\pi(\Gamma_h + \Gamma_e)(\sigma_h^{xy} - \sigma_e^{xy})}{\Gamma_h D_e^{xx} + \Gamma_e D_h^{xx}}$$

$$\times (\sigma_h^{xy} - \sigma_e^{xy}),$$

vanishes for a compensated system. In this case, the formally weaker contribution of the recombination surface layer determines the field dependence of the conductivity

$$\overline{\sigma}_s \approx \frac{2}{\kappa_2 W} \frac{(\Gamma_h D_e^{xx}\sigma_h^{xy} + \Gamma_e D_h^{xx}\sigma_e^{xy})(D_h^{xy} D_e^{xx} + D_e^{xy} D_h^{xx})}{(\Gamma_h D_e^{xx} + \Gamma_e D_h^{xx})D_e^{xx} D_h^{xx}},$$
$$(109)$$

which is linear in the magnetic field.

We conclude that compensated 3D systems with the geometry of Fig. 5 exhibit linear magnetoresistance when subjected to the perpendicular magnetic field.

B. Oblique magnetic field

Consider now the general situation where the magnetic field is not collinear with any sample edges, see Fig. 5. In this section we restrict ourselves to the electron-hole symmetric system at charge neutrality. In this case, the macroscopic equation describing transport properties of the system can be simplified similarly to the 2D case.

In the geometry of Fig. 5 and under the assumption $d \gg W$, all physical quantities depend only on the coordinate y. Hence the continuity equation for the total quasiparticle flow, $\boldsymbol{P} = (0, P_y(y), P_z(y))$, takes the form [cf. Eq. (25c)]

$$P_y' = -\delta\rho/\tau_R. \quad (110a)$$

The equations expressing the relation between the quasiparticle flows and the electric field [cf. Eqs. (38), (90), and (98)] can be expressed in terms of the total quasiparticle flow and the electric current (96):

$$D \begin{pmatrix} \delta\rho' \\ 0 \end{pmatrix} + \begin{pmatrix} P_y \\ P_z \end{pmatrix} + j\tau \begin{pmatrix} \omega_z \\ -\omega_y \end{pmatrix} = 0, \quad (110b)$$

$$j - eE_0\rho_0\tau/m + \tau(P_z\omega_y - P_y\omega_z) = 0, \quad (110c)$$

where $\omega_{y(z)} = eB_{y(z)}/mc$.

Solving the equations (110) with the hard wall boundary conditions, $P_y(y = \pm W/2) = 0$, we find

$$P_y(y) = \frac{j_0\omega_z\tau}{1 + \tau^2\omega_c^2} \left[\frac{\cosh \lambda y}{\cosh(\lambda W/2)} - 1 \right],$$

and

$$j(y) = \frac{j_0}{1 + \tau^2\omega_c^2} \left[1 + \frac{\omega_z^2\tau^2}{1 + \omega_y^2\tau^2} \frac{\cosh \lambda y}{\cosh(\lambda W/2)} \right].$$

Here $j_0 = eE_0\rho_0\tau/m$ is the electric current in the absence of the magnetic field, $\omega_c^2 = \omega_y^2 + \omega_z^2$, and λ is the inverse field-dependent "recombination length",

$$\lambda^2 = \frac{1}{D\tau_R}\left[1 + \frac{\tau^2\omega_z^2}{1 + \tau^2\omega_y^2}\right].$$

The resulting averaged resistance of the sample is calculated similarly to the case of the orthogonal geometry and has the form

$$R_\square = \frac{m}{e^2\rho_0\tau}\frac{1 + \tau^2\omega_c^2}{1 + \frac{\tau^2\omega_z^2}{1+\tau^2\omega_y^2}F(\lambda W/2)}, \qquad (111)$$

where, as defined above, $F(x) = \tanh x/x$.

In narrow samples, $\lambda W \ll 1$, recombination is ineffective since the time it takes the carriers to move from one slab facet to another is smaller than the typical recombination (as well as diffusion) time. Nevertheless, in contrast to the above case of the orthogonal geometry the magnetoresistance is nonzero,

$$R_\square = \rho_0(1 + \tau^2\omega_y^2),$$

and is determined by the y-component of the magnetic field. The physical reason fro this result is the effect of the magnetic field on carrier motion in the z-direction.

In wide samples,

$$\lambda W \gg \tau^2\omega_z^2/(1 + \tau^2\omega_y^2),$$

we recover the classical bulk magnetoresistance, which is quadratic in the applied magnetic field:

$$R_\square = \varrho_0[1 + \tau^2\omega_c^2].$$

This result can also be obtained within the Drude theory of two-component systems if the electric current is allowed to flow only in the x-direction.

Finally, one may consider the intermediate situation:

$$1 \ll \lambda W \ll \tau^2\omega_z^2/(1 + \tau^2\omega_y^2). \qquad (112)$$

Such an interval may only exist when the direction of the magnetic field is almost orthogonal to the sample face: $\omega_z \gg \omega_y$ or, equivalently, $\theta \ll 1$. Then the sample resistance takes the form:

$$R_\square = \frac{\rho_0 W}{2\sqrt{D\tau_R}}\frac{[1 + \tau^2\omega_y^2]^{1/2}[1 + \tau^2\omega_c^2]^{3/2}}{\tau^2\omega_z^2}. \qquad (113)$$

Using $\omega_z\tau \gg 1$ and $\omega_y \ll \omega_z$, the above expression can be simplified to

$$R_\square = \rho_0(W/\ell_0)\tau\omega_z\sqrt{1 + \tau^2\omega_y^2}. \qquad (114)$$

The resistance (114) exhibits an approximately linear field dependence if $\tau\omega_y \ll 1$, such that the square root may be approximate by unity. In a general situation the magnetoresistance is quadratic, see Fig. 6.
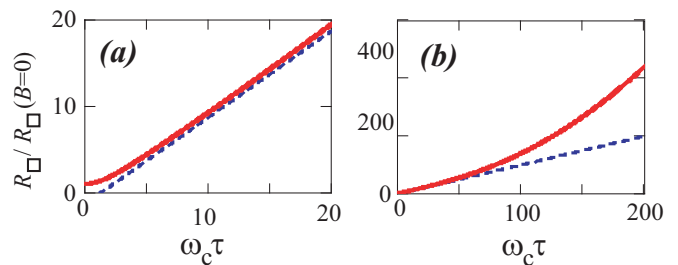

FIG. 6: (Color online) 3D two-component system at charge neutrality in an oblique magnetic field. The recombination length in zero magnetic field is taken to be equal to the sheet width: $W/\ell_0 = 1$. The solid red curves represent the calculated values of the magnetoresistance. The field is directed at the angle $\theta = 0.5^o$. The two panels show the same result in the two different ranges of the parameter $\omega_c\tau$: the panel (a) shows the onset of the intermediate, nearly linear behavior, while the panel (b) shows the recovery of the quadratic magnetoresistance in strong fields. The dashed blue lines are guides to the eye.

IV. CONCLUSIONS

In this paper, we have studied the recombination mechanism of magnetoresistance in finite-size, two-component systems near charge neutrality[84]. Precisely at the neutrality point the classical Hall effect is compensated. In particular, there is no Hall voltage. The electric current flowing through the system is accompanied by a lateral, neutral quasiparticle flow. In any finite-size system (i.e. in any sample studied in laboratory experiments) this flow terminates at the boundary leading to quasiparticle accumulation in the well-defined edge region, see Fig. 1. The width of that region is determined by inelastic scattering processes and is of the order of the recombination length. The latter depends on the external magnetic field and hence the edge region contributes to the overall magnetoresistance of the sample. The relative strength of this contribution (as compared to the bulk of the system) depends on the sample geometry, strength of the recombination processes, and magnetic field. In strong enough magnetic fields, there exist a wide region of parameters, where the edge contribution dominates over the bulk leading to the linear dependence of the sample resistance on the external field.

Our explicit calculations show that the recombination mechanism of LMR in compensated two-component systems is generic and independent of the details of the quasiparticle excitation spectrum. Away from the neutrality point, the linear field dependence eventually saturates at the strongest (but still classical) fields. Such strong dependence of the magnetoresistance on the carrier density distinguishes the recombination mechanism from the previously proposed extreme quantum[85–87] and classical[77–79] theories.

Magnetoresistance observed in experiments on compensated two-component systems[34,36] does exhibit the
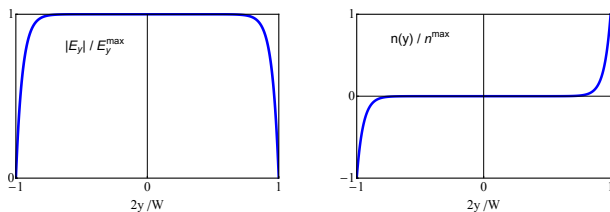
FIG. 7: Spatial profiles of the lateral electric field (left) and charge density (right) in the classical Hall effect in a sample with the slab geometry of Fig. 5.

essential qualitative features of the recombination mechanism. At the same time, LMR is observed in a wide variety of materials, many of which do not conform to the assumptions of the present paper. It is therefore very interesting to extend the theory of recombination-assisted magnetoresistance in two-component materials to the cases of strongly disordered systems (including the long-wavelength, smooth disorder), systems where recombination processes are mostly effective near the boundaries, and situations where the electron-phonon coupling is not strong enough to provide a mechanism for fast energy relaxation and thermalization.

Appendix: Screening boundary layer in the classical Hall effect

Here we discuss the boundary layer in the classical Hall effect in disordered metals with *finite conductivity*. In contrast to the textbook case of an ideal conductor, here the charges are not confined to the boundary and the electric field is nonzero inside the metal.

The electric current density, $\boldsymbol{J}$, inside a metal is related to the electric field and charge density by means of Ohm's law [cf. Eq. (38)],

$$\boldsymbol{J} = \hat{\sigma}\boldsymbol{E} - e\hat{D}(B)\boldsymbol{\nabla}n, \tag{A.1}$$

where n denotes the *volume density* of charge carriers, such that en is the charge density. In the presence of the magnetic field, the diffusion coefficient is represented by the matrix

$$\hat{D}(B) = \frac{D}{1 + \omega_c^2\tau^2}\begin{pmatrix} 1 & \omega_c\tau \\ \omega_c\tau & 1 \end{pmatrix},$$

see Eq. (40). In a steady state, we may write the continuity equation as [cf. Eq. (25c)]

$$\boldsymbol{\nabla} \cdot \boldsymbol{J} = 0. \tag{A.2}$$

Finally, the electric field and charge density are related by Maxwell's equation,

$$\boldsymbol{\nabla} \cdot \boldsymbol{E} = 4\pi en. \tag{A.3}$$

Taking the gradient of Eq. (A.1) and using Eqs. (A.2) and (A.3), one finds

$$\boldsymbol{\nabla} \cdot (\hat{\sigma}\boldsymbol{E}) = e\boldsymbol{\nabla} \cdot \left(\hat{D}\boldsymbol{\nabla}n\right). \tag{A.4}$$

Solution to the coupled differential equations (A.3) and (A.4) depends on the system geometry.

Assuming the simplest geometry of Fig. 5, we may exclude the electric field from Eqs. (A.3) and (A.4). This way we find the equation[105] for the carrier density $n(y)$ [cf. Eqs. (42), (64), and (101)],

$$n'' = 4\varkappa^2 n, \tag{A.5}$$

where $\varkappa$ is the inverse Thomas-Fermi screening length, $\varkappa = \sqrt{\pi\sigma^{xx}(B=0)/D}$ (assuming $\sigma^{yy} = \sigma^{xx}$).

Solving Eq. (A.5) with the hard wall boundary conditions[2] [cf. Eqs. (24) and (102b)]

$$J^y(\pm W/2) = 0, \qquad E_y(\pm W/2) = 0, \tag{A.6}$$

we find the carrier density profile

$$n(y) = \frac{\sigma^{yx}E_0}{2e\varkappa D^{yy}}\frac{\sinh 2\varkappa y}{\cosh \varkappa W}. \tag{A.7}$$

The lateral component of the electric field is given by

$$E_y(y) = \frac{\pi\sigma^{yx}E_0}{\varkappa^2 D^{yy}}\left(\frac{\cosh 2\varkappa y}{\cosh \varkappa W} - 1\right). \tag{A.8}$$

These results are illustrated in Fig. 7. Clearly, the off-diagonal component of the conductivity matrix, $\sigma^{yx} \propto B$, is nonzero only in the presence of the external magnetic field. Both the charge density and electric field are non-uniform close to the sample boundaries. The width of the corresponding boundary layer is determined by the screening length. In an ideal conductor, the screening length is equal to zero. In this limit, the charge density (A.7) develops a singularity at the boundary corresponding to the *surface* charge density [which in turn leads to the jump of the lateral electric field at the boundary[2] in contrast with the boundary condition (A.6)].

Substituting the results (A.7) and (A.8) into Eq. (A.1), we recover the usual field-independent resistance, typical for single-component systems[1–3].

[1] A.B. Pippard, *Magnetoresistance in Metals* (Cambridge University Press, Cambridge, UK, 1989).

[2] L.D. Landau and E.M. Lifshitz, and L. P. Pitaevskii, *Electrodynamics of Continuous Media* (Pergamon, NY, 1984).

[3] A.A. Abrikosov, *Fundamentals of the Theory of Metals* (North-Holland, Amsterdam, 1988).

[4] C. Kittel, *Quantum Theory of Solids* (Wiley, NY, 1963).

[5] P.L. Kapitza, Proc. R. Soc. London A **119**, 358 (1928).

[6] K.S. Novoselov, A.K. Geim, S.V. Morozov, D. Jiang, Y. Zhang, S.V. Dubonos, I.V. Grigorieva, and A.A. Firsov, Science **306**, 666 (2004).

[7] K.S. Novoselov, D. Jiang, T. Booth, V.V. Khotkevich, S.M. Morozov, and A.K. Geim, PNAS **102**, 10451 (2005).

[8] A.K. Geim and K.S. Novoselov, Nature Mat. **6**, 183 (2007).

[9] A.K. Geim, Science **324**, 1530 (2009).

[10] K.S. Novoselov, Rev. Mod. Phys. **83**, 837 (2011).

[11] A.K. Geim, Rev. Mod. Phys. **83**, 851 (2011).

[12] B.A. Bernevig, T.A. Hughes, and S.C. Zhang, Science **314**, 1757 (2006).

[13] L. Fu and C.L. Kane, Phys. Rev. B **76**, 045302 (2007).

[14] M. König, S. Wiedmann, C. Brne, A. Roth, H. Buhmann, L.W. Molenkamp, X.L. Qi and S.C. Zhang, Science **318**, 766 (2007).

[15] D. Hsieh, D. Qian, L. Wray, Y. Xia, Y.S. Hor, R.J. Cava, and M.Z. Hasan, Nature **452**, 970 (2008).

[16] Y. Xia, D. Qian, D. Hsieh, L. Wray, A. Pal, H. Lin, A. Bansil, D. Grauer, Y.S. Hor, R.J. Cava, and M.Z. Hasan, Nature Phys. **5**, 398 (2009).

[17] Z.K. Liu, B. Zhou, Y. Zhang, Z.J. Wang, H.M. Weng, D. Prabhakaran, S.-K. Mo, Z.X. Shen, Z. Fang, X. Dai, Z. Hussain, and Y.L. Chen, Science **343**, 864 (2014).

[18] M. Neupane, S.-Y. Xu, R. Sankar, N. Alidoust, G. Bian, C. Liu, I. Belopolski, T.-R. Chang, H.-T. Jeng, H. Lin, A. Bansil, F. Chou, and M.Z. Hasan, Nature Communications **5**, 3786 (2014).

[19] S. Borisenko, Q. Gibson, D. Evtushinsky, V. Zabolotnyy, B. Büchner, and R.J. Cava, Phys. Rev. Lett. **113**, 027603 (2014).

[20] S.-Y. Xu, I. Belopolski, N. Alidoust, M. Neupane, C. Zhang, R. Sankar, S.-M. Huang, C.-C. Lee, G. Chang, B. Wang, G. Bian, H. Zheng, D.S. Sanchez, F. Chou, H. Lin, S. Jia, and M.Z. Hasan, Science **349**, 613 (2015).

[21] B.Q. Lv, H.M. Weng, B.B. Fu, X.P. Wang, H. Miao, J. Ma, P. Richard, X.C. Huang, L.X. Zhao, G.F. Chen, Z. Fang, X. Dai, T. Qian, and H. Ding, Phys. Rev. X **5**, 031013 (2015).

[22] S.-Y. Xu, C. Liu, S.K. Kushwaha, R. Sankar, J.W. Krizan, I. Belopolski, M. Neupane, G. Bian, N. Alidoust, T.-R. Chang, H.-T. Jeng, C.-Y. Huang, W.-F. Tsai, H. Lin, P.P. Shibayev, F.-C. Chou, R.J. Cava, and M.Z. Hasan, Science **347**, 294 (2015).

[23] L. Lu, Z. Wang, D. Ye, L. Ran, L. Fu, J.D. Joannopoulos, and M. Soljačić, Science **349**, 622 (2015).

[24] B.Q. Lv, N. Xu, H.M. Weng, J.Z. Ma, P. Richard, X.C. Huang, L.X. Zhao, G.F. Chen, C. Matt, F. Bisti, V. Strokov, J. Mesot, Z. Fang, X. Dai, T. Qian, M. Shi, and H. Ding, Nature Phys. **11**, 724 (2015).

[25] S.-Y. Xu, N. Alidoust, I. Belopolski, C. Zhang, G. Bian, T.-R. Chang, H. Zheng, V. Strokov, D.S. Sanchez, G. Chang, Z. Yuan, D. Mou, Y. Wu, L. Huang, C.-C. Lee, S.-

[26] M. Huang, B. Wang, A. Bansil, H.-T. Jeng, T. Neupert, A. Kaminski, H. Lin, S. Jia, and M.Z. Hasan, Nature Physics **11**, 748 (2015).

[26] Y. Pan, H. Wang, P. Lu, J. Sun, B. Wang, and D.Y. Xing, arXiv:1509.03975 (2015).

[27] Q. Li, D.E. Kharzeev, C. Zhang, Y. Huang, I. Pletikosic, A.V. Fedorov, R.D. Zhong, J.A. Schneeloch, G.D. Gu, and T. Valla, Nature Phys. (2016)

[28] A.L. Friedman, J.L. Tedesco, P.M. Campbell, J.C. Culbertson, E. Aifer, F.K. Perkins, R.L. Myers-Ward, J.K. Hite, C.R. Eddy, G.G. Jernigan, and D.K. Gaskill, Nano Lett. **10**, 3962 (2010).

[29] R.S. Singh, X. Wang, W.C. Ariando, and A.T.S. Wee, App. Phys. Lett. **101**, 183105 (2012).

[30] M. Veldhorst, M. Snelder, M. Hoek, C.G. Molenaar, D.P. Leusink, A.A. Golubov, H. Hilgenkamp, and A. Brinkman, Phys. Status Solidi RRL **7**, 26 (2013).

[31] W. Wang, Y. Du, G. Xu, X. Zhang, E. Liu, Z. Liu, Y. Shi, J. Chen, G. Wu, and X. Zhang, Sci. Rep. **3**, 2181 (2013).

[32] G. M. Gusev, E. B. Olshanetsky, Z. D. Kvon, N. N. Mikhailov, and S. A. Dvoretsky, Phys. Rev. B **87**, 081311 (R) (2013).

[33] F. Kisslinger, C. Ott, C. Heide, E. Kampert, B. Butz, E. Spiecker, S. Shallcross, and H. B. Weber, Nature Phys. **11**, 650 (2015).

[34] S. Wiedmann, A. Jost, C. Thienel, C. Brüne, P. Leubner, H. Buhmann, L.W. Molenkamp, J.C. Maan, and U. Zeitler, Phys. Rev. B **91**, 205311 (2015).

[35] C.M. Wang and X.L. Lei, Phys. Rev. B **92**, 125303 (2015).

[36] G.Yu. Vasileva, D. Smirnov, Yu.L. Ivanov, Yu.B. Vasilyev, P.S. Alekseev, A.P. Dmitriev, I.V. Gornyi, V.Yu. Kachorovskii, M. Titov, B.N. Narozhny, and R.J. Haug, Phys. Rev. B **93**, 195430 (2016).

[37] J. Hu and T.F. Rosenbaum, Nature Mat. **7**, 698 (2008).

[38] F.Y. Yang, K. Liu, K. Hong, D.H. Reich, P.C. Searson, and C.L. Chien, Science **284**, 1335 (1999).

[39] F.Y. Yang, K. Liu, K. Hong, D.H. Reich, P.C. Searson, C.L. Chien, Y. Leprince-Wang, KuiYu-Zhang, and K. Han, Phys. Rev. B **61**, 6631 (2000).

[40] R. Xu, A. Husmann, T.F. Rosenbaum, M.-L. Saboungi, J.E. Enderby, and P.B. Littlewood, Nature **57**, 390 (1997).

[41] A. Husmann, J.B. Betts, G.S. Boebinger, A. Migliori, T.F. Rosenbaum, and M.-L. Saboungi, Nature **417**, 421 (2002).

[42] Y. Sun, M.B. Salamon, M. Lee, and T.F. Rosenbaum, Appl. Phys. Lett. **82**, 1440 (2003).

[43] M.N. Ali, J. Xiong, S. Flynn, Q. Gibson, L. Schoop, N. Haldolaarachchige, N.P. Ong, J. Tao, and R.J. Cava, Nature **514**, 205 (2014).

[44] I. Pletikosic, M.N. Ali, A.V. Fedorov, R.J. Cava, and T. Valla, Phys. Rev. Lett. **113**, 216601 (2014).

[45] Y. Luo, H. Li, Y.M. Dai, H. Miao, Y.G. Shi, H. Ding, A.J. Taylor, D.A. Yarotski, R.P. Prasankumar, and J.D. Thompson, Appl. Phys. Lett. **107**, 182411 (2015).

[46] C. Shekhar, A.K. Nayak, Y. Sun, M. Schmidt, M. Nicklas, I. Leermakers, U. Zeitler, Z. Liu, Y. Chen, W. Schnelle, J. Grin, C. Felser, and B. Yan, Nature Physics **11**, 645 (2015).

[47] N. Kumar, C. Shekhar, S.-C. Wu, I. Leermakers, O. Young, U. Zeitler, B. Yan, and C. Felser, Phys. Rev. B

93, 241106 (2016).

[48] P.J. Guo, H.C. Yang, B.J. Zhang, K. Liu, Z.Y. Lu, Phys. Rev. B **93**, 235142 ((2016).

[49] R. Singha, A. Pariari, B. Satpati, and P. Mandal, arXiv: 1602.01993 (2016).

[50] Y.-Y. Lv, B.-B. Zhang, X. Li, S.-H. Yao, Y.B. Chen, J. Zhou, S.-T. Zhang, M.-H. Lu, and Y.-F. Chen, Appl. Phys. Lett. **108**, 244101 (2016).

[51] K. Gopinadhan, Y.J. Shin, R. Jalil, T. Venkatesan, A.K. Geim, A.H. Castro Neto, and H. Yang, Nature Comm. **6**, 8337 (2015).

[52] K. Wang, D. Graf, and C. Petrovic, Sci. Rep. **4**, 7328 (2014).

[53] Z. Hou, Y. Wang, E. Liu, H. Zhang, W. Wang, and G. Wu, Appl. Phys. Lett. **107** (2015).

[54] T. Liang, Q. Gibson, M.N. Ali, M. Liu, R.J. Cava, and N.P. Ong, Nature Materials **14**, 280 (2015) .

[55] Y.Y. Wang, Q.H. Yu, P.J. Guo, K. Liu, and T.L. Xia, Phys. Rev. B **94**, 041103 (2016).

[56] X. Wang, Y. Du, S. Dou, and C. Zhang, Phys. Rev. Lett. **108**, 266806 (2012).

[57] O. Pavlosiuk, D. Kaczorowski, and P. Wisniewski, Sci. Rep. **5**, 9158 (2015).

[58] X. Zhang, Q.Z. Xue, and D.D. Zhu, Phys. Lett. A **320**, 471 (2004).

[59] F. Arnold, C. Shekhar, S.-C. Wu, Y. Sun, R.D. dos Reis, N. Kumar, M. Naumann, M.O. Ajeesh, M. Schmidt, A.G. Grushin, J.H. Bardarson, M. Baenitz, D. Sokolov, H. Borrmann, M. Nicklas, C. Felser, E. Hassinger, and B. Yan, Nature Comm. **7**, 11615 (2015).

[60] X. Yang, Y. Liu, Z. Wang, Y. Zheng, Z.-an. Xu, arXiv: 1506.03190 (2015).

[61] M. Diez, A.M.R.V.L. Monteiro, G. Mattoni, E. Cobanera, T. Hyart, E. Mulazimoglu, N. Bovenzi, C.W.J. Beenakker, and A.D. Caviglia, Phys. Rev. Lett. **115**, 016803 (2015).

[62] X.L. Wang, Q. Shao, A. Zhuravlyova, M. He, Y. Yi, R. Lortz, J.N. Wang, and A. Ruotolo, Sci. Rep. **5**, 9221 (2015).

[63] H. Li, H. He, H.-Z. Lu, H. Zhang, H. Liu, R. Ma, Z. Fan, S.-Q. Shen, J. Wang, Nature Comm. **7**, 10301 (2016).

[64] M.V. Yakunin, A.V. Suslov, M.R. Popov, E.G. Novik, S.A. Dvoretsky, N.N. Mikhailov, Phys. Rev. B **93**, 085308 (2016).

[65] C. Zhang, S.-Y. Xu, I. Belopolski, Z. Yuan, Z. Lin, B. Tong, N. Alidoust, C.-C. Lee, S.-M. Huang, T.-R. Chang, H.-T. Jeng, H. Lin, M. Neupane, D.S. Sanchez, H. Zheng, G. Bian, J. Wang, C. Zhang, H.-Z. Lu, S.-Q. Shen, T. Neupert, M.Z. Hasan, and S. Jia, Nature Comm. 7, 10735 (2016).

[66] Y. Luo, R.D. McDonald, P.F.S. Rosa, B.Scott, N. Wakeham, N.J. Ghimire, E.D. Bauer, J.D. Thompson, and F. Ronning, Sci. Rep. **6**, 27294 (2016).

[67] Y. Li, L. Li, J. Wang, T. Wang, X. Xu, C. Xi, C. Cao, J. Dai, arXiv:1601.02062 (2016).

[68] Y. Li, Z. Wang, Y. Lu, X. Yang, Z. Shen, F. Sheng, C. Feng, Y. Zheng, and Z.-A. Xu, arXiv:1603.04056 (2016).

[69] A.A. Burkov, J. Phys.: Cond. Mat. **27**, 113201 (2015).

[70] A. Lucas, R.A. Davison, and S. Sachdev, PNAS **113**, 9463 (2016).

[71] S.D. Ganichev, H. Ketterl, W. Prettl, I.A. Merkulov, V.I. Perel, I.N. Yassievich, and A.V. Malyshev, Phys. Rev. B **63**, 201204(R) (2001).

[72] P.S. Alekseev, Phys. Rev. Lett. **117**, 166601 (2016).

[73] H. Weiss and H. Welker, Z. Phys. **138**, 322 (1954).

[74] V.F. Gantmakher and Y.B. Levinson, Zh. Eksp. Teor. Fiz. **74**, 261 (1978) [Sov. Phys. JETP **47**, 133 (1978)]; *Carrier Scattering in Metals and Semiconductors* (North-Holland, Amsterdam, 1987).

[75] M.Y. Azbel, Zh. Eksp. Teor. Fiz. 44, 983 (1963) [Sov. Phys. JETP 17, 667 (1963)].

[76] I.M. Lifshitz, M.Y. Azbel, and M.I. Kaganov, *Electron Theory of Metals* (Consultants Bureau, New York, 1973).

[77] A.M. Dykhne, Sov. Phys. JETP **32**, 348 (1971) [Zh. Eksp. Teor. Fiz. **59**, 641 (1970)].

[78] M.M. Parish and P.B. Littlewood, Nature **426**, 162 (2003).

[79] M. Knap, J.D. Sau, B.I. Halperin, and E. Demler, Phys. Rev. Lett. **113**, 186801 (2014).

[80] F. Kisslinger, C. Ott, and H.B. Weber, Phys. Rev. B **95**, 024204 (2017) .

[81] K. Yoshida, J. Phys. Soc. Jpn. **41**, 574 (1976); J. Appl. Phys. **50**, 4159 (1979); J. Appl. Phys. **51**, 4226 (1980).

[82] D.G. Polyakov, Sov. Phys. JETP **63**,(1986) [Zh. Eksp. Teor. Fiz. **90**, 546 (1986)].

[83] J.C.W. Song, G. Refael, and P.A. Lee, Phys. Rev. B 92, 180204 (2015)

[84] P.S. Alekseev, A.P. Dmitriev, I.V. Gornyi, V.Y. Kachorovskii, B.N. Narozhny, M. Schütt, M. Titov, Phys. Rev. Lett. **114**, 156601 (2015).

[85] A.A. Abrikosov, Sov. Phys. JETP **29**, 746 (1969) [Sov. Phys. JETP **29**, 746 (1969)].

[86] A.A. Abrikosov, Phys. Rev. B **58**, 2788 (1998).

[87] A.A. Abrikosov, Europhys. Lett. **49**, 789 (2000).

[88] G. Zala, B.N. Narozhny, and I.L. Aleiner, Phys. Rev. B **65**, 020201 (2001).

[89] J. Klier, I.V. Gornyi, and A.D. Mirlin, Phys. Rev. B **92**, 205113 (2015).

[90] M. Titov, R. V. Gorbachev, B. N. Narozhny, T. Tudorovskiy, M. Schütt, P.M. Ostrovsky, I.V. Gornyi, A.D. Mirlin, M.I. Katsnelson, K.S. Novoselov, A.K. Geim, and L.A. Ponomarenko, Phys. Rev. Lett. **111**, 166601 (2013).

[91] B.N. Narozhny and A. Levchenko, Rev. Mod. Phys. **88**, 025003 (2016).

[92] E.I. Rashba, Z.S. Gribnikov, and V.Ya. Kravchenko, Sov. Phys. Usp. **19**, 361 (1976) [Usp. Fiz. Nauk **119**, 3 (1976)].

[93] Note, that LMR may also appear in short samples[94], see also Ref. 80 as well as the earlier work[81]. Such effects are beyond the scope of the present paper.

[94] S. Lakeou, S. Cristoloveanu, and A. Chovet, Phys. Stat. Sol. (a) **43**, 213 (1977).

[95] S.-J. Chang, M. Bawedin, and S. Cristoloveanu, IEEE Trans. Electr. Dev. **61**, 1979 (2014).

[96] G.A. Brooker and J. Sykes, Annals of Physics, **56**, 1 (1970).

[97] U. Briskot, M. Schütt, I.V. Gornyi, M. Titov, B.N. Narozhny, and A.D. Mirlin, Phys. Rev. B **92**, 115426 (2015).

[98] B.N. Narozhny, I.V. Gornyi, M. Titov, M. Schütt, and A. D. Mirlin, Phys. Rev. B **91**, 035414 (2015).

[99] A.B. Kashuba, Phys. Rev. B **78**, 085415 (2008).

[100] L. Fritz, J. Schmalian, M. Müller, and S. Sachdev, Phys. Rev. B **78**, 085416 (2008).

[101] M.S. Foster and I.L. Aleiner, Phys. Rev. B **79**, 085415 (2009).

[102] M. Schütt, P.M. Ostrovsky, I.V. Gornyi, and A.D. Mirlin, Phys. Rev. B **83**, 155441 (2011).

[103] D. Svintsov, V. Vyurkov, S. Yurchenko, T. Otsuji, and V. Ryzhii, J. Appl. Phys. **111**, 083715 (2012).

[104] D. Svintsov, V. Vyurkov, V. Ryzhii, and T. Otsuji, Phys. Rev. B **88**, 245444 (2013).

[105] A. Shik, J. Phys. Cond. Matt. **5**, 8963 (1993).